Research and Development of Large-Aperture Hybrid Photo-Detectors for Hyper-Kamiokande

Yusuke Suda
Department of Physics, University of Tokyo

January 7, 2014

Abstract

We have developed the prototype of the 8-inch Hybrid Photo-Detector (HPD) and the high quantum efficiency (QE) 20-inch photomultiplier tube (PMT) for Hyper-Kamiokande (Hyper-K) which is proposed as a next generation Megaton class water Cherenkov detector. Our goal is to develop the high-QE 20-inch HPD which satisfies the requirements to photosensors in Hyper-K.

We evaluated the performance of the 8-inch HPD. The timing resolution for single photoelectron, the single photocelectron charge resolution, and the dark rate at 0.5 photoelectron threshold are measured to be 1.2 ns (1 σ), 12 %, and 2 kHz, respectively.

To ensure the usability of HPD and high-QE PMT, we evaluate the performance in a 200 ton water tank as a sensor for a water Cherenkov detector. For the test in the tank, we checked the durability and safety in water of the 8-inch HPD. No trouble has been found. We calibrated the gain of the sensors before installation. Then, we installed eight 8-inch HPDs, five high-QE PMTs and 227 normal-QE PMTs into the tank. The installation of the sensors is successfully completed and the cosmic muon events were observed in the tank. The single photoelectron resolution of the 8-inch HPD in the tank is better than that of PMT. Because of the low temperature in the tank and closing the tank for two months, the dark rate of the 8-inch HPD decreases. The dark rate of the high-QE PMTs measured in the tank is comparable to that of the normal ones. This is the first time to operate HPD and sensor which has a high-QE photocathode as a sensor for a water Cherenkov detecter.

Through the test in the tank and more precise measurement, we plan to decide the photosensors for Hyper-K in 2016.

Contents

Chapter 1

Introduction

In this thesis, we report the performance of 8-inch Hybrid Photo-Detector (HPD) and the test in a 200-ton water Cherenkov detector. The performance of high quantum efficiency (QE) 20-inch photomultiplier tube (PMT) is also presented. These are developed for Hyper-Kamiokande (Hyper-K), which is proposed as a next generation Megaton class water Cherenkov detector [1].

The road to new physics is opened by the discovery of neutrino oscillation in the atmospheric neutrino by Super-Kamiokande in 1998 [2]. Since then, many experiments to explore neutrino oscillation parameters have been conducted. Recently, the last mixing angle θ_{13} has been measured by T2K [3], Daya Bay [4], RENO [5] and Double Chooz [6]. Non-zero θ_{13} opens the opportunity to measure the CP phase δ in the lepton sector which is the last neutrino oscillation parameter. Other than that, there are many Grand Unified Theories (GUTs) proposed as beyond the standard models. Most GUTs predict nucleon decays. Super-Kamiokande has found no evidence of nucleon decays. Astrophysics using a supernova burst neutrino and a solar neutrino is needed to study the life of star. For these study, Hyper-K is strongly desired.

We have been developing the high-QE 20-inch HPD as a photosensor for Hyper-K detector. HPDs are much simpler in structure and have better performance than PMTs. In order to detect as many photons as possible, the sensor is desired to have as high quantum efficiency as possible. As a first step, we have developed the prototype of 8-inch HPD and the high-QE venetian blind dynode 20-inch PMT. Through the R&D of these sensors, we evaluate HPD and high-QE technique and give a feedback to the development of the high-QE 20-inch HPD. In this thesis, the status of photosensor R&D for Hyper-Kamiokande is presented.

Our physics targets and overview of Hyper-K are presented in Chapter 2. The requirements to photosensors, overview of our R&D and the principle and system of 8-inch HPD are shown in Chapter 3. In Chapter 4, we describe the performance evaluation of 8-inch HPD. We conduct the test in a 200-ton water Cherenkov detector to evaluate the performance of new photosensors as the sensor for a water Cherenkov detector. Overview of the test, some preparation, the installation and the measurement in the tank are discussed in Chapter 5. We summarize our study and explain the future prospect of our R&D in Chapter 6.

Chapter 2

Physics motivation

In this chapter, we describe the physics motivation for the Hyper-Kamiokande project and what we need to realize the Hyper-Kamiokande.

2.1 Physics targets

We briefly explain the physics targets of Hyper-Kamiokande.

2.1.1 Neutrino oscillation

Here we describe the neutrino oscillation phenomenon. Assuming that neutrinos have finite masses and the flavor eigenstates of neutrinos are different from the mass eigenstates of neutrinos, the flavor eigenstates are expressed as:

$$|\nu_\alpha\rangle = \sum_i U_{MNS}^{\alpha i} |\nu_i\rangle \,, \tag{2.1}$$

where $|\nu_\alpha\rangle\,(\alpha = e, \mu, \tau)$ is the flavor eigenstate, $|\nu_i\rangle\,(i = 1, 2, 3)$ is the mass eigenstate, and $U_{MNS}^{\alpha i}$ is an element of the 3×3 unitary matrix called the MNS (Maki-Nakagawa-Sakata) matrix [7]. The MNS matrix is expressed with four independent parameters:

$$U_{MNS} = \begin{pmatrix} 1 & 0 & 0 \\ 0 & c_{23} & s_{23} \\ 0 & -s_{23} & c_{23} \end{pmatrix} \begin{pmatrix} c_{13} & 0 & s_{13}e^{-i\delta} \\ 0 & 1 & 0 \\ -s_{13}e^{i\delta} & 0 & c_{13} \end{pmatrix} \begin{pmatrix} c_{12} & s_{12} & 0 \\ -s_{12} & c_{12} & 0 \\ 0 & 0 & 1 \end{pmatrix} \tag{2.2}$$

$$= \begin{pmatrix} c_{12}c_{13} & s_{12}c_{13} & s_{13}e^{-i\delta} \\ -s_{12}c_{23} - c_{12}s_{23}s_{13}e^{i\delta} & c_{12}c_{23} - s_{12}s_{23}s_{13}e^{i\delta} & s_{23}c_{13} \\ s_{12}s_{23} - c_{12}c_{23}s_{13}e^{i\delta} & -c_{12}s_{23} - s_{12}c_{23}s_{13}e^{i\delta} & c_{23}c_{13} \end{pmatrix}, \tag{2.3}$$

where θ is a mixing angle, $c_{ij} = \cos\theta_{ij}$, $s_{ij} = \sin\theta_{ij}$ and δ is a CP violating phase. CP violation in the lepton sector occurs if $\delta \neq 0$. For the simplicity, here we consider two neutrino flavors ν_α and ν_β, and two neutrino mass eigenstates ν_1 and ν_2. We can rewrite Eq. 2.3 with a mixing angle θ:

$$\begin{pmatrix} |\nu_\alpha\rangle \\ |\nu_\beta\rangle \end{pmatrix} = U \begin{pmatrix} |\nu_1\rangle \\ |\nu_2\rangle \end{pmatrix} = \begin{pmatrix} \cos\theta & \sin\theta \\ -\sin\theta & \cos\theta \end{pmatrix} \begin{pmatrix} |\nu_1\rangle \\ |\nu_2\rangle \end{pmatrix}. \tag{2.4}$$

In vacuum, the time evolution of the mass eigenstate is given as follows:

$$|\nu_i(t)\rangle = e^{-i(E_i t - p_i x)} |\nu_i(0)\rangle \tag{2.5}$$

where E_i and p_i are the energy and momentum of ν_i. Assuming that the neutrino are highly relativistic:

$$t = \frac{L}{v} \approx \frac{L}{c} = L, p_i = \sqrt{E_i^2 - m_i^2} \approx E_i - \frac{m_i^2}{2E_i}, \tag{2.6}$$

where L is the position of the neutrino. Eq. 2.4 is written as:

$$\begin{pmatrix} |\nu_\alpha(L)\rangle \\ |\nu_\beta(L)\rangle \end{pmatrix} = U \begin{pmatrix} e^{-i\frac{m_1^2 L}{2E_1}} & 0 \\ 0 & e^{-i\frac{m_2^2 L}{2E_2}} \end{pmatrix} U^{-1} \begin{pmatrix} |\nu_\alpha(0)\rangle \\ |\nu_\beta(0)\rangle \end{pmatrix}. \tag{2.7}$$

We can calculate the oscillation probability between two flavors as follows:

$$\begin{aligned} P(\nu_\alpha \to \nu_\beta) &= |\langle \nu_\beta(0)|\nu_\alpha(L)\rangle|^2 & (2.8) \\ &= \sin^2 2\theta \sin^2\left(\frac{\Delta m_{21}^2 L}{4E}\right) & (2.9) \\ &= \sin^2 2\theta \sin^2\left(\frac{1.27\Delta m_{21}^2(\mathrm{eV}^2)L(\mathrm{km})}{E(\mathrm{GeV})}\right), & (2.10) \end{aligned}$$

where $\Delta m_{21}^2 = m_2^2 - m_1^2$ and we use $E = E_1 \approx E_2$. If neutrino oscillation occurs, at least one of neutrinos has finite mass.

The finite mass of neutrino is not included in the standard model of the elementary particle. In 1998, Super-Kamiokande (Super-K) experiment discovered the neutrino oscillation with the measurement of the atmospheric neutrinos. This is the first evidence that the new physics exists.

To build up the beyond the standard model, we want to know all of the elements of the MNS matrix. These elements can be measured by the neutrino oscillation.

2.1.2 Leptonic CP violation

Now, we know the approximate value of all mixing angles, θ_{23}, θ_{12} and θ_{13}. Only one parameter in the MNS matrix, the CP phase δ is still unknown. We have an opportunity to measure the δ thanks to the large angle of θ_{13}. CP violation in the lepton sector may be a key to solve the problem of the matter-antimatter asymmetry in our universe.

The effect of the CP phase appears in the difference between the transition probabilities $P(\nu_\alpha \to \nu_\beta)$ and $P(\bar{\nu}_\alpha \to \bar{\nu}_\beta)$. The most promising channel to detect the difference in transition probabilities is $\nu_\mu(\bar{\nu}_\mu) \to \nu_e(\bar{\nu}_e)$. Accelerator-based neutrino oscillation experiment can measure these two channels. T2K (Tokai to Kamioka) experiment and NOvA (NuMI Off-Axis ν_e Appearance) experiment [8] are the accelerator-based neutrino oscillation experiments. In T2K, the $\nu_\mu(\bar{\nu}_\mu)$ beam is produced by the J-PARC accelerator located in Tokai-mura, shooting them into the Super-K and detect them. We expect that the full sensitivity of the CP phase combined with the result of reactor neutrino experiments is around 2σ.

To determine the CP phase, we need more statistics of neutrino events than that of T2K expected. A larger volume water Cherenkov detector than Super-K and higher intensity neutrino beam are strongly required.

2.1.3 Nucleon decay

Grand Unified Theories (GUTs) are proposed as a candidate of a framework beyond the standard model. GUTs unify the strong and electroweak forces. Most GUTs allow baryon number violating interactions and predict nucleon decays.

Super-Kamiokande has been searching for the nucleon decays such as $p \to e^+ + \pi^0$ and $p \to \bar{\nu}K^+$ since 1996. Super-K is the largest detector for the observation of nucleon decay in the world. But no evidence has been found in Super-K. The current limit of proton partial lifetime is 1.4×10^{34} years for $p \to e^+ + \pi^0$.

One of GUTs, SUSY SO(10), predicts that the limit of proton lifetime is order 10^{35} years. To detect the nucleon decay and determine GUTs, we need a larger detector than Super-K.

2.1.4 Astrophysics using neutrinos

At the end of life of massive stars, they explode and emit many neutrinos called the supernova burst neutrinos. The energy of the supernova burst neutrinos is expected to be about 10$\sim$30 MeV. The observation of the supernova burst neutrinos gives us a clue to explore the mechanism of supernova explosion. On the 23rd of February 1987, the Kamiokande II [9], IMB [10] and Baksan [11] experiments observed the supernova burst neutrinos from SN1987A located in the Large Magellanic Cloud. Neutrino astronomy starts from this discovery. Unfortunately, no supernova explosion has been observed since the neutrino burst of SN1987A. But, recently, it is said that Betelgeuse might be explode and emit the supernova burst neutrinos.

The neutrino from the sun produced by the process of the nuclear fusion is called the solar neutrino. The energy of the solar neutrinos is below 20 MeV. By observing the solar neutrino, we can study the state of inside the sun in real time. The standard solar model is tested by the observation of the solar neutrinos.

To detect the supernova burst neutrinos and the solar neutrinos as many as possible, we need a large detector which can be observe MeV order neutrino.

2.2 The principle of water Cherenkov detectors

Super-K is one of water Cherenkov detectors. Water Cherenkov detectors mainly consist of a tank to store water and many photosensors on the wall of the tank. When a charged particle travels faster than the speed of light in the water, it emits Cherenkov light. The Cherenkov light propagates at a constant angle θ specific to the velocity of the charged particle, which is written as:

$$\cos\theta = \frac{1}{\beta n}, \tag{2.11}$$

where β is the speed of the charged particle in unit of c and $n = 1.33$ is the refractive index of water (Fig. 2.1). The number of Cherenkov photons dN generated per unit distance the charged particle travels dx per unit wavelength $d\lambda$ is calculate as:

$$\frac{d^2N}{dxd\lambda} = \frac{2\pi\alpha}{\lambda^2}\left(1 - \frac{1}{n^2\beta^2}\right), \tag{2.12}$$

where α is the fine structure constant. If we use Super-K PMT which is sensitive to the wavelength range of 300 $\sim$ 600 nm in a water Cherenkov detector, the number of observable Cherenkov photons is about 340 in water per 1 cm track length for the charged particle which has a unit charge and velocity of $\beta \approx 1$. The emission of Cherenkov photons keeps on until the energy of the charged particle E becomes as:

$$E_{thr} = \frac{m}{\sqrt{1-(\frac{v}{c})^2}} = \frac{nm}{\sqrt{n^2-1}}, \tag{2.13}$$

where m is the mass of the charged particle. For electron, E_{thr} should be 0.78 MeV. We can roughly calculate the number of Cherenkov photons induced by a 10 MeV electron is about 1500 photons. In Super-K II which has photocoverage 20 %, the light yield is about 2.8 photoelectrons/MeV. The photo-coverage and the quantum efficiency of the photosensor are critical for the study of low energy neutrino.

The photosensors detect a ring image of the Cherenkov light. From the timing and the total amount of light, we can identify the particle and reconstruct the energy momentum vector of the particle. When a neutrino comes from outside the tank, it might interact with H_2O. Then, a corresponding charged lepton is produced via charged current interaction. Using the photosensors, we can detect the neutrino. Electron- and muon-like event can be distinguished by the shape of the Cherenkov ring. In case of electron-like event, it will be smeared by the cascade shower.

The major advantage of to use water Cherenkov detectors is that it is easier to prepare a target (water) with large effective volume than other detectors such as liquid scintillators or liquid argon time projection chambers.

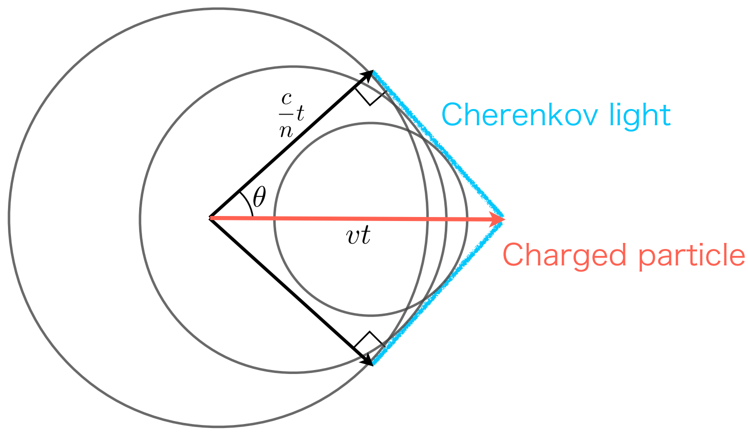

Figure 2.1: Sketch of that the charged particle which travels faster than the speed of light emits the Cherenkov light in water.

2.3 Hyper-Kamiokande project

A larger water Cherenkov detector is needed for more precise measurement of neutrino oscillation parameters, the measurement of CP asymmetry, search for nucleon decay, the observation of the supernova burst neutrino and the solar neutrino and so on. For that purpose, Hyper-Kamiokande (Hyper-K) detector is proposed as a next generation underground water Cherenkov detector.

Hyper-K has 0.99 (0.56) Megaton total (fiducial) mass, which is about 20 (25) times larger than that of Super-Kamiokande (Fig. 2.2) [12]. The candidate site is Kamioka mine, Gifu, Japan. There are a lot of pure water and hard bedrocks in Kamioka mine. It is suitable to construct a Megaton class water Cherenkov detector. Figure 2.3 shows a cross section of Hyper-K tank. The tank consists of an inner detector and an outer detector. The outer detector is a veto part for cosmic muon. In the inner detector, we need 99,000 20-inch photosensors. Also in the outer detector, 25,000 8-inch photosensors are needed. The photo-coverage which indicates a photosensitive area in the inner tank is 20 %. This is half photo-coverage of that of Super-K.

Since we need huge number of photosensors, the R&D of new photosensors is critical to the Hyper-Kamiokande project.

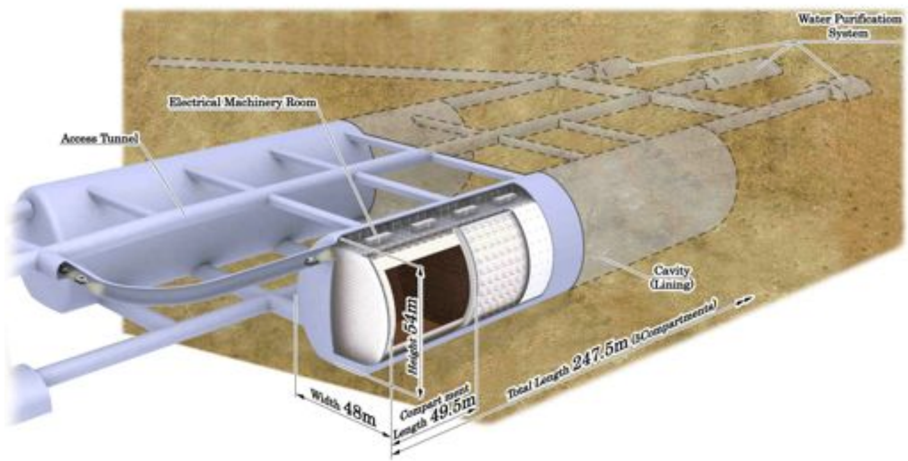

Figure 2.2: Hyper-Kamiokande detector [1].

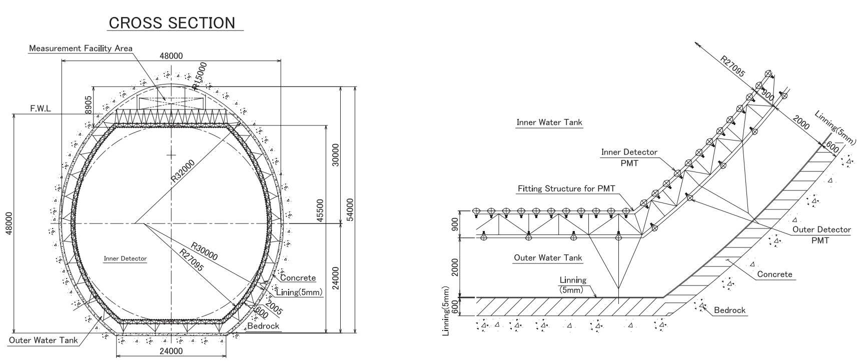

Figure 2.3: Cross section of Hyper-Kamiokande detector [1].

Chapter 3

Photosensor R&D for Hyper-Kamiokande

3.1 Requirements to photosensors in Hyper-K

Major requirements to photosensors in Hyper-K are as follows:

Good timing resolution
: Timing resolution is essential to reconstruct the vertex of neutrino interaction. Considering the transit time spread (TTS) of the single photoelectron of PMTs used in Super-K is 2.2 ns, we require the TTS of the single photoelectron of the photosensor for Hyper-K to be better than 2.2 ns.

High single photoelectron sensitivity
: In order to observe a low energy neutrino event which is induced by a MeV order neutrino, the photosensor needs high single photoelectron sensitivity. We require the single photoelectron resolution of the photosensor for Hyper-K to be better than that of Super-K PMT 60 %.

Large photosensitive area
: This is required to achieve good energy resolution.

High Quantum Efficiency (QE)
: In order to detect as many photons as possible, the photosensor is desired to have as high quantum efficiency as possible.

Low dark rate
: From the point of view of the data acquisition (DAQ) system and low energy physics capability, the dark rate of a photosensor must be less than ~ 4 kHz.

Wide dynamic range
: In order to study very high energy event, a dynamic range up to $\sim$ 1000 photoelectrons is required.

High rate tolerance

In order to record a supernova burst neutrino event without event loss, the sensor needs to be capable of handling high rate signal up to 1 MHz.

Simple structure

High assembling precision of photosensors and high productivity are expected with a simple structure. This is important for cost reduction in mass production because we need 0.1 million photosensors.

The sensitivity of the $p \rightarrow \bar{\nu}K^+$ event will be improved if the timing resolution of new photosensors became better than Super-K PMT. In the $p \rightarrow \bar{\nu}K^+$ event, a proton in ^{16}O decays as follows:

$$^{16}O \rightarrow {}^{15}N + \gamma + \bar{\nu} + K^+ \tag{3.1}$$
$$K^+ \rightarrow \nu_\mu + \mu^+ \tag{3.2}$$
$$\mu^+ \rightarrow \bar{\nu}_\mu + \nu_e + e^+. \tag{3.3}$$

Excited ^{15}N emits 6 MeV γ. The ring image induced by this γ is not clear ring because 6 MeV γ rings not many photosensors. K^+ stops and decays into μ^+ and $\bar{\nu}_\mu$. The momentum of μ^+ is expected to be 236 MeV/c. The muon stops and decays into e^+, $\bar{\nu}_\mu$ and ν_e. We can identify μ and e clearly. There are three peaks in the hit timing distribution when the $p \rightarrow \bar{\nu}K^+$ event occurs. First is γ peak, second is μ^+ peak and final is e^+ peak. To tag γ, TTS of photosensors should be small. The timing resolution of photosensors is crucial for the search of the $p \rightarrow \bar{\nu}K^+$ event.

3.2 R&D of the Hyper-K photosensors

In this section, we explain the three candidates of Hyper-K photosensor, the goal, schedule and the status of our R&D.

3.2.1 Candidate photosensors

There are three photosensors as candidates for photosensors in Hyper-K as follows.

Venetian Blind dynode type PMT (R3600)

This is employed in Super-K. The performance is well confirmed.

Box&Line dynode type PMT

This is a new type of PMT which has a better timing resolution than R3600.

Large-Aperture Hybrid Photo-Detector (HPD)

An HPD uses avalanche diode instead of dynodes to multiply the photoelectrons. The development of HPD is the main topic of this thesis.

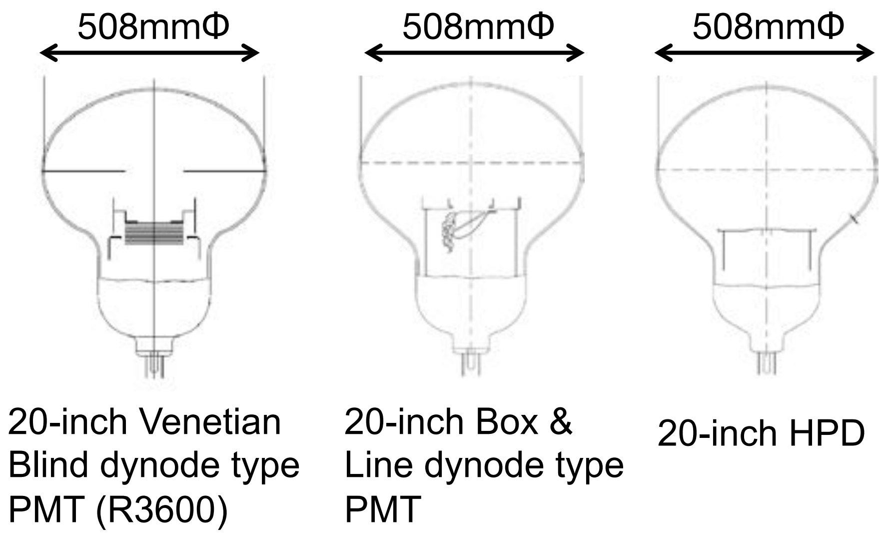

Figure 3.1: Three candidates of Hyper-K photosensors.

Figure 3.1 shows the drawings of three candidates. The major difference between HPDs and PMTs is that HPDs substitute avalanche diode for dynodes in PMTs to multiply the photoelectrons. Because of the difference, HPDs are much simpler in structure, have a better timing resolution and better resolution of single photoelectron than PMTs. Table 3.1 shows the comparison of each photosensor. Transit time spread (TTS) is an index of the timing resolution.

3.2.2 High-QE photocathode development

As a common option for three candidates, we have been developing a high-QE photocathode. Hamamatsu Photonics K.K. has recently developed a high-QE R3600 which has 30 % QE, 1.5 times larger than that of Super-K PMT (normal-QE R3600). The QE spectra as a function of wavelength for eight high-QE R3600s and a typical value of normal-QE PMTs are shown in Fig. 3.2. First, we evaluate the high-QE R3600. Then, we apply this high-QE technique to other candidates of Hyper-K photosensor.

3.2.3 Schedule

Figure 3.3 shows a schedule of R&D of photosensors. To select the Hyper-K photosensor, we have to verify the performance and usability of the box&line PMTs, HPDs and high-QE R3600s. We evaluate the basic performance of each photosensor. Then, we will test the usability of photosensors for Hyper-K in a 200-ton water Cherenkov detector for 1 $\sim$ 2 years. Before starting the test,

Table 3.1: The comparison of performance of candidate photosensors. $*$ indicates the circulated value.

20-inch type	Venetian Blind PMT	Box&Line PMT	HPD
HV	2kV	2kV	8kV
Gain	10^7	10^7	10^{4-5}
TTS (FWHM)	$\sim$5.5 ns	$\sim$ 2.7 ns*	$\sim$0.75 ns*
Collection Efficiency*	80%	93%	95%

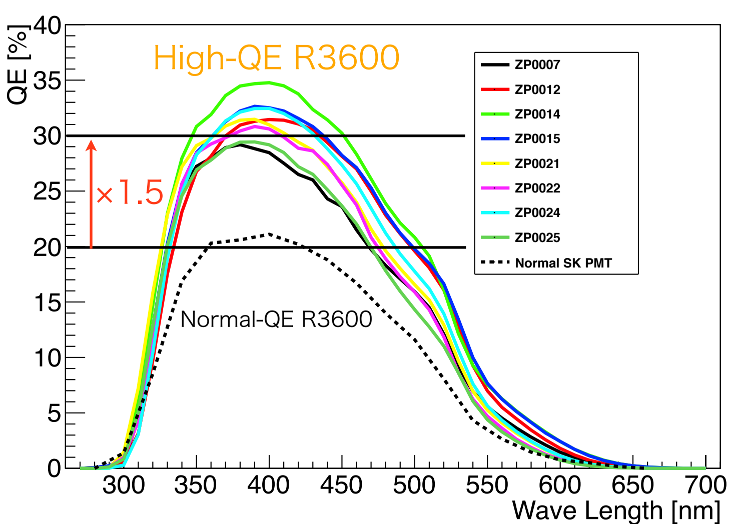

Figure 3.2: QE vs. wavelength for high-QE and normal-QE R3600.

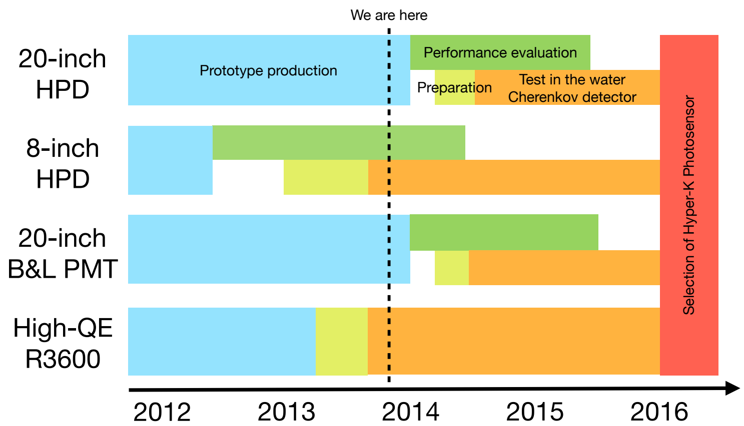

Figure 3.3: Schedule of R&D of Hyper-K photosensors.

we have some preparation such as pre-calibration, safety check and installation. The detailed performance evaluation is carried out in parallel with the test in the water Cherenkov detector. We plan to decide the photosensors for Hyper-K in 2016.

3.3 Hybrid Photo-Detector

In this section, we describe the principle of HPD and the design of 8-inch HPD system which we are currently using.

3.3.1 The principle of HPD

The HPD consists of a phototube and an avalanche diode (AD). AD is a kind of semiconductor device. Figure 3.4 shows the principle of our HPD. An electron produced by photoelectric effect is accelerated by a high electric field ($\sim$ 8kV) from the photocathode to the AD. Many electron-ion pairs are created inside the AD via the ionization loss of the bombardment electron. We obtain the bombardment gain $\sim 1,600$. Then, electrons and ions are amplified by a AD bias voltage, giving the avalanche gain $30 \sim 100$. With the two multiplication mechanisms, the HPD realizes a gain of order 10^5.

3.3.2 The 8-inch HPD system used in this thesis

The HPD used for the study described in this thesis is equipped with a preamplifier and a high voltage (HV) module inside the housing as shown in Fig. 3.5. Figure 3.6 shows pictures of an 8-inch HPD without any equipment. A picture of the 5mmϕ AD which is used in 8-inch HPD is shown in Fig. 3.7.

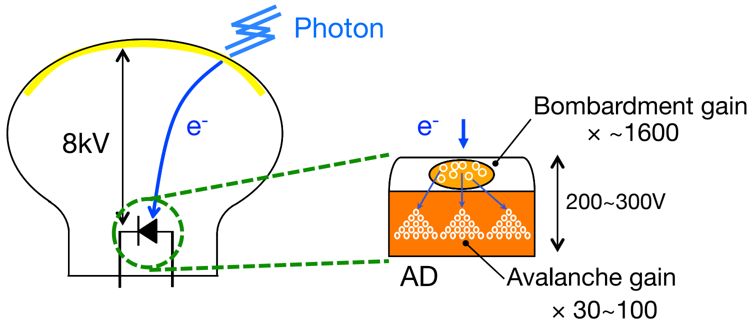

Figure 3.4: Principle of HPDs.

Figure 3.8 shows a schematic diagram of the circuit inside an HPD. The HV module made by CAEN produces two voltages; One is the high voltage applied between the photocathode and the AD. The other is the bias voltage of the AD. Usually, we apply the HV 8kV and the AD bias voltage around 300 V. The operation of the HPD in water is safe because we do not need a HV cable in water. The specification of the HV module is shown in Table 3.2. We put filters between the AD and the HV module to eliminate high frequency noise coming from the HV module. A protection device against electric discharge such as a varistor is placed in next to the decoupling capacitor. We employ an I-V inverted differential amplifier as a preamplifier to eliminate common mode noise coming from the AD. A raw signal of AD is a positive polarity. For convenience to use HPDs in the same condition as PMTs, it is better to invert the raw signal. The specification of the preamplifier is shown in Table 3.3. After a decoupling capacitor which is placed in the end of preamplifier, we get the signal of the 8-inch HPD.

To control the HV and the AD bias voltage, we use a control power supply shown in Fig. 3.9. This power supply has four functions; One is to apply 10 V as the power of the HV module and the preamplifier. Second is to control the HV and the AD bias via changing the HV control voltage and the AD bias control voltage. Monitoring the over current of the HV module, if it occurred, a LED lamp turns red. The other one is transmission of the signal from HPD to the DAQ system. The specification of the control power supply is shown in Table 3.4.

3.4 Goals of this thesis

The most desirable solution to Hyper-K photosensor is to develop the high-QE 20-inch HPD which satisfy the requirements to photosensors in Hyper-K because it is expected to have better performance than the other options. But there is no large-aperture HPD which can be used in water Cherenkov detector.

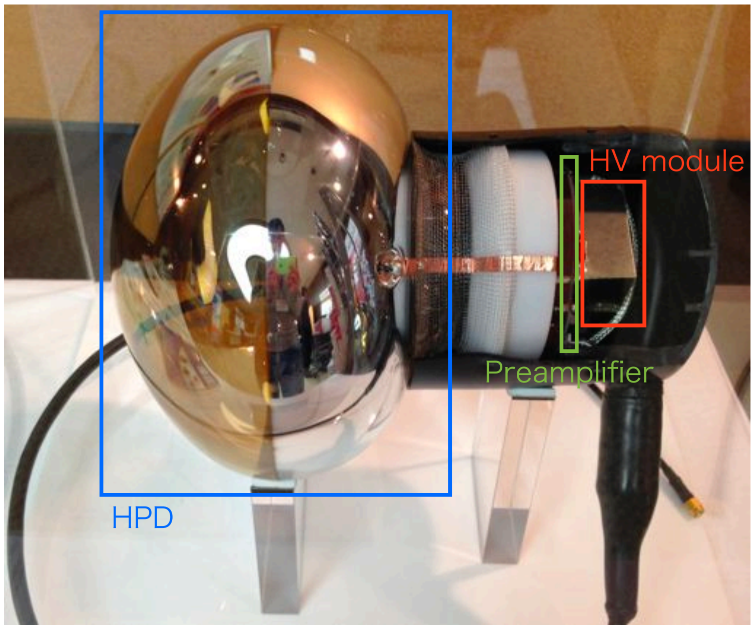

Figure 3.5: Picture of 8-inch HPD.

Figure 3.6: Picture of 8-inch HPD. The front view (left) and the top view(right).

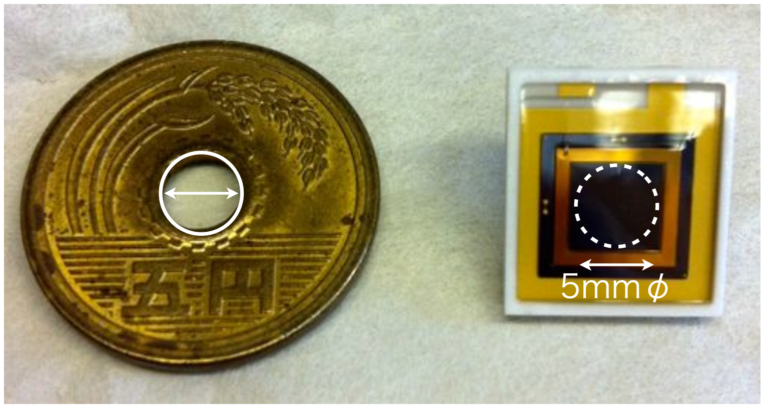

Figure 3.7: Picture of 5mmϕ avalanche diode.

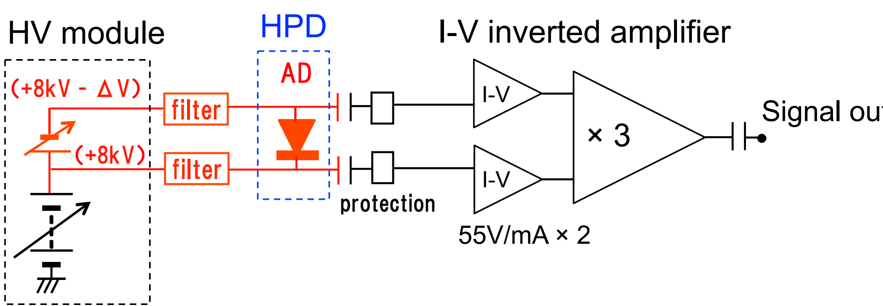

Figure 3.8: Schematic view of the circuit inside HPD.

Table 3.2: Specification of the HV module produced by CAEN.

Item	Value
Output voltage	0∼10 kV for HV 0∼500 V for AD bias voltage
Supply voltage	5 V
Current	∼ 120 mA
Control voltage for HV and AD bias voltage	0 ∼ 4
Enable voltage	5 V (on) / 0 V (off)

Table 3.3: Specification of the preamplifier.

Item	Value
Band width	25 MHz
Gain	54 kV/A
Supply voltage	5 V
Current	$\sim$ 15 mA
Output impedance	50 Ω

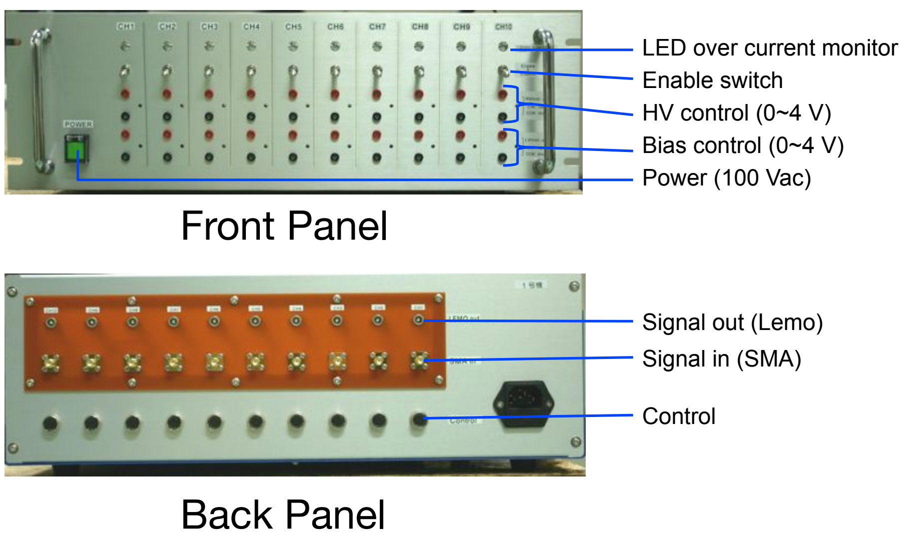

Figure 3.9: Pictures of the control power supply.

Table 3.4: Specification of the control power supply.

Item	Value
Output voltage	10 V for HV module and preamplifier 0$\sim$4 V for HV and AD bias control voltage
Supply voltage	100 Vac

Thus, we need to develop a new sensor for Hyper-K. As a first step, we have developed the prototype of 8-inch HPD with QE $\sim$20% and the high-QE R3600 in cooperation with Hamamatsu Photonics K.K. Through the R&D of these sensors, we evaluate HPD and high-QE technique and give a feedback to the development of the high-QE 20-inch HPD. Moreover, the 8-inch HPD has a possibility to be the photosensor for the outer detector of Hyper-K. For that reason, the R&D of the 8-inch HPD and the high-QE R3600 is an important step for Hyper-K.

In this thesis, we present the measured performance of the 8-inch HPDs. After checking the performance of the 8-inch HPD, we prepare for the test in the water Cherenkov detector. The measurement including the high-QE R3600s in the water tank will be presented and compared with the result measured before installation.

Chapter 4

Performance evaluation of 8-inch HPD

The performance of 8-inch HPD with the preamplifier is described in this chapter.

4.1 Output signal

Figure 4.1 shows the typical output signal of 8-inch HPD with the applied HV of 8 kV and AD bias voltage of 300 V. We use Hamamatsu high-repetition picosecond light pulsar (PLP, model PLP-10, λ = 405 nm, pulse width 70 ps (typ.)), NIM standard clock module and an oscilloscope (LeCroy, wave runner 104MXi). The HPD has excellent capability of single photon detection compared with PMTs. The rise time of the HPD with the preamplifier is around 10 ns and the pulse width is around 60 ns. Due to the bandwidth of the preamplifier, the time response of the signal becomes worse. An HPD without preamplifier has the rise time $\sim$1.7 ns and the fall time $\sim$2.7 ns.

4.2 Total Gain

Figure 4.2 schematically shows the setup for the gain measurement. We use PLP and VME standard ADC module (CAEN mod. V265). The input light intensity is set to many photoelectrons level which is regarded as Gaussian distribution in charge. The charge of the output was measured by the charge integrating ADC with 200 ns gate width. The gain is defined by (sigma of Gaussian)^2/{(mean of Gaussian)$\times$(electric charge)}. Figure 4.3 shows the gain curve with fixed HV of 8 kV. The total gain of the 8-inch HPD with the preamplifier is $(2 \sim 5) \times 10^7$.

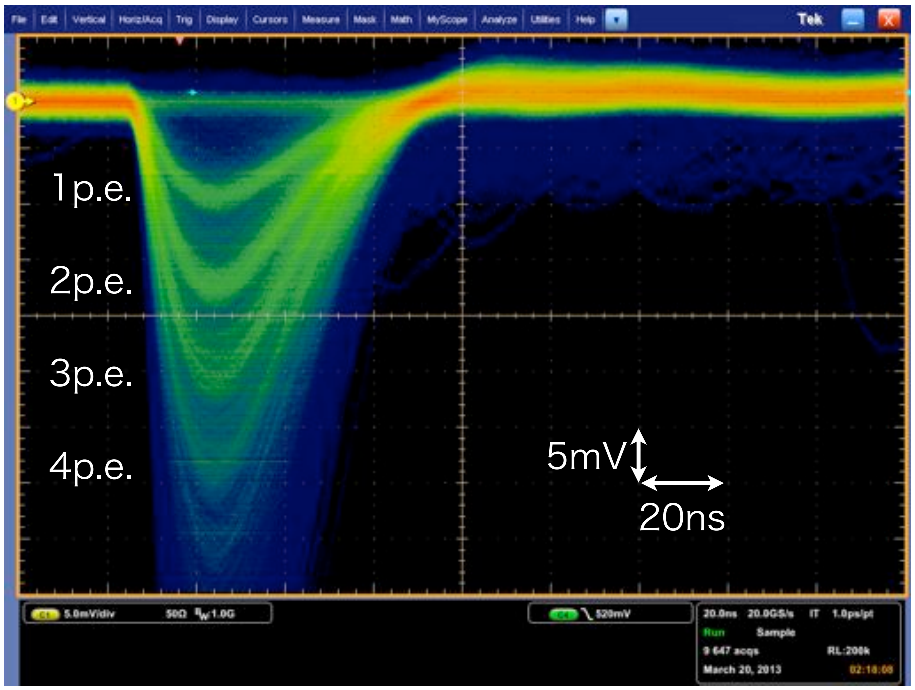

Figure 4.1: Typical waveform of 8-inch HPD with the preamplifier.

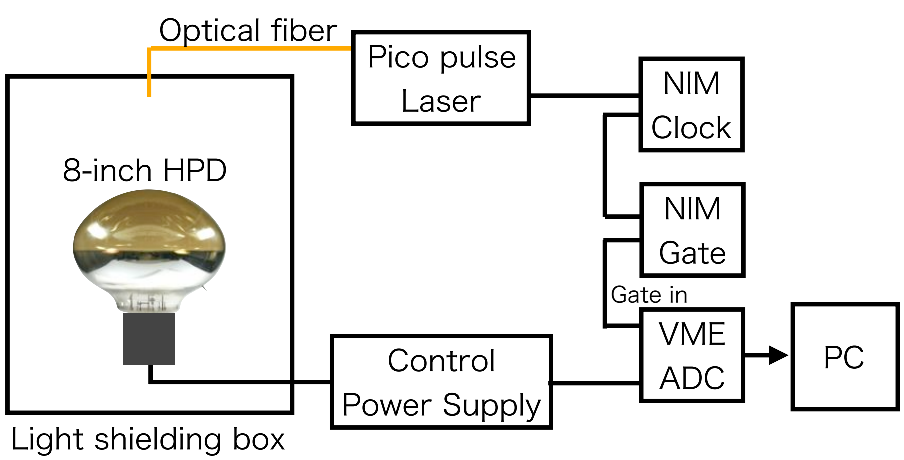

Figure 4.2: Schematic view of the setup for the measurement of the output charge.

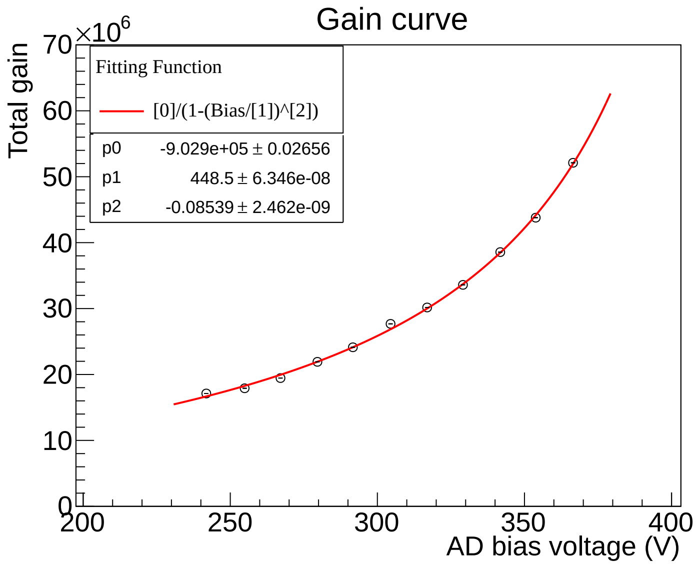

Figure 4.3: Total gain as a function of the AD bias voltage with fixed HV of 8 kV.

4.3 Dark rate

The dark rate is measured as a function of threshold. In this measurement, we use two Analog Timing Module (ATM) boards (Fig. 4.4). ATM is a DAQ board which was used in Super-K I, II and III. A detailed description for ATM can be found elsewhere [13]. ATM can count up the hit and attenuate the input pulse. The hit is defined by the signal which exceeds the threshold level. The range of the threshold is from 0 mV to 12.5 mV. The pulse height of a single photoelectron signal from an HPD is about 15 mV at this time. The first ATM is used to attenuate the pulse height of HPD to 10 % of its original value and send it to the second ATM. The second ATM counts the hit by varying the threshold level. The temperature of measurement place is 24 °C.

Figure 4.5 shows the measured dark rate of 8-inch HPD. The dark rate is 2kHz at 0.5 photoelectron. The typical dark rate of Super-K PMT is ∼4kHz with 0.25 photoelectron threshold. When used in a water Cherenkov detector, the dark rate of 8-inch HPD is expected to decrease with operation time in the dark environment and with lower temperature (13 °C) in the water tank. It will be checked by the long term test in the water tank described in Chapter 5.

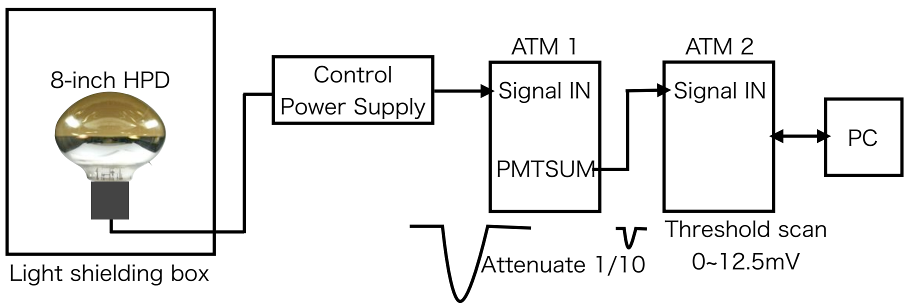

Figure 4.4: Schematic view of the setup of dark rate measurement.

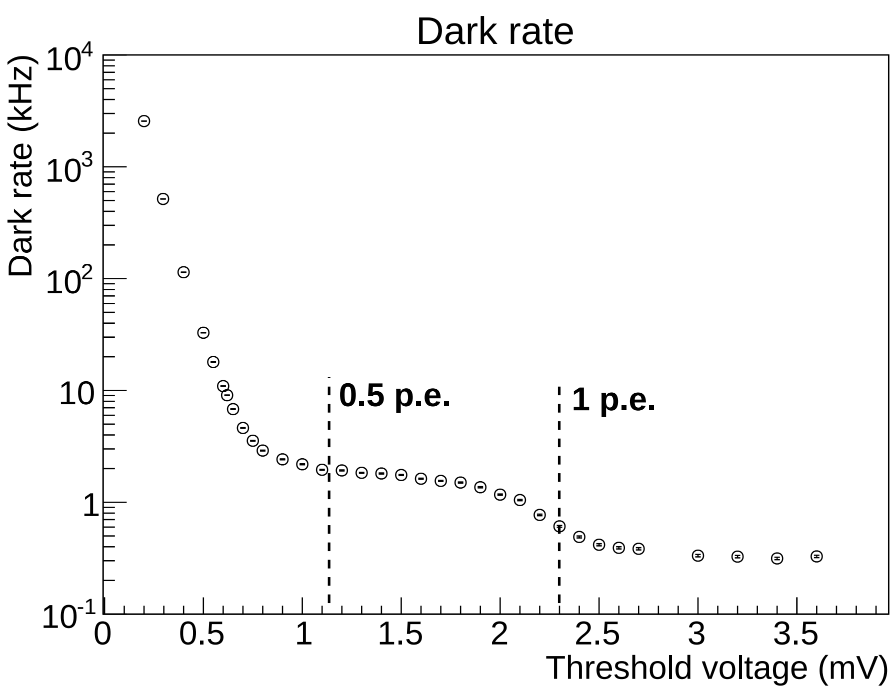

Figure 4.5: Dark rate as a function of the threshold.

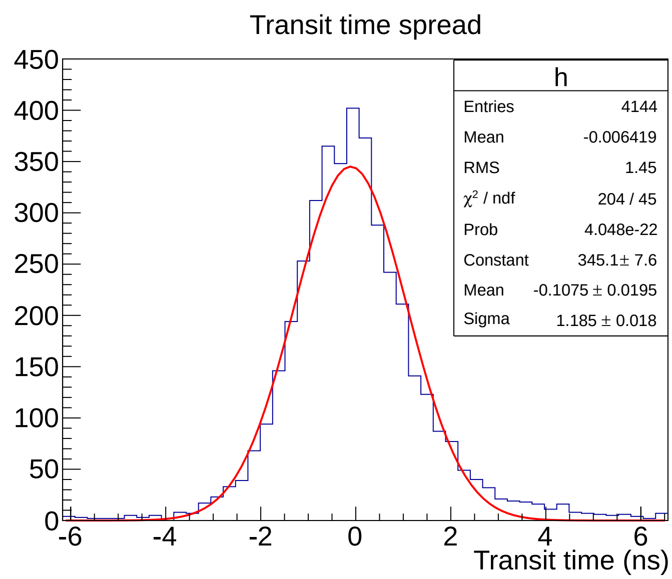

Figure 4.6: Transit time distribution of single photoelectron.

4.4 Timing resolution

We evaluate the transit time spread (TTS) as a measure of timing resolution. The definition of the transit time is the time from a trigger of a light source to 25 % pulse height of signal. To measure TTS, we record the waveforms of 8-inch HPD using an oscilloscope and analyze them offline. We define TTS as a sigma of the Gaussian function fitted to the histogram of the transit time. TTS of an HPD is around 1.2 ns in sigma as shown in Fig. 4.6. Note that this HPD's TTS includes not only TTS of the HPD itself, but also that of the preamplifier. An HPD itself has 0.62 ns TTS. Thanks to the absence of dynodes, the TTS of an HPD is better than that for Super-K PMT (2.2 ns in sigma) [14], although the sensor sizes are different. We expect the TTS of 8-inch HPD will be improved with the optimization of the preamplifier. Figure 4.7 shows TTS vs. number of input photoelectrons. TTS gets smaller by increasing the number of photoelectrons.

4.5 Charge distribution

We measure the charge distribution with the same setup shown in Fig. 4.2. The gate width of the ADC is 200 ns. The charge distribution with single photoelectron level light input is shown in Fig. 4.8. The flat region between the pedestal peak and the single photoelectron peak is presumed to be due to electrons backscattered on the surface of AD. To evaluate the mean and sigma

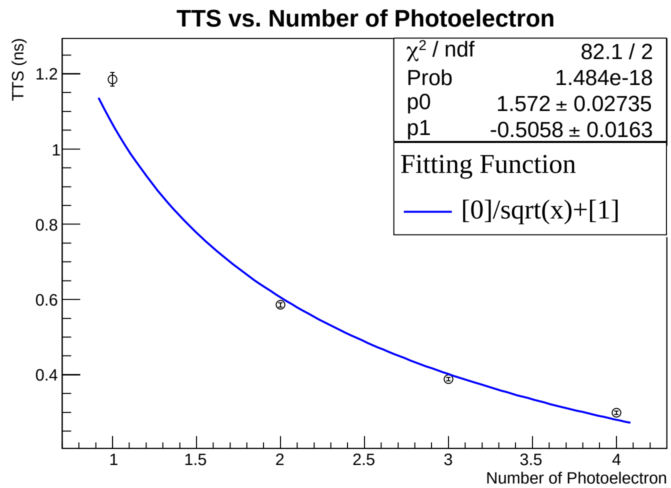

Figure 4.7: TTS as a function of a function of the number of input photoelectrons.

of the pedestal and single photoelectron, we employ a composite function which consists of two Gaussian and an error function. The error function is used to take account of the effect of the backscattering.

An 8-inch HPD has 12 % single photoelectron resolution defined by (sigma of single photoelectron peak)/(mean of single photoelectron peak). We evaluate the signal to noise (S/N) ratio which is an index of the significance of separation of the single photoelectron from the noise level of pedestal. The S/N ratio is given by (mean of single photoelectron peak)/(sigma of pedestal peak). For this HPD, the S/N ratio is 12. We also evaluate the peak-to-valley (P/V) ratio. It is defined as a ratio of the charge of single photoelectron peak to the valley between the pedestal peak and the single photoelectron peak. The P/V ratio is around 5.6. On the other hand, Super-K PMT has around 60 % single photoelectron resolution in sigma, the S/N ratio of about 2.2 and the P/V ratio of 1.9 [14]. An HPD has better single photoelectron resolution, the S/N ratio and the P/V ratio than Super-K PMT. The charge distribution for multi photoelectrons is shown in Figure 4.9. Clear photoelectron peak can be seen up to four photoelectrons.

4.6 Rate tolerance

We measure the response of an 8-inch HPD to high rate input by changing the light emission frequency of the laser diode (Fig. 4.2). Figure 4.10 shows the measured output charge as a function of input light frequency with three different light intensity. HPD has rate tolerance up to 500 kHz within 5 % variation. The rate tolerance of the current HPD is limited by the response of

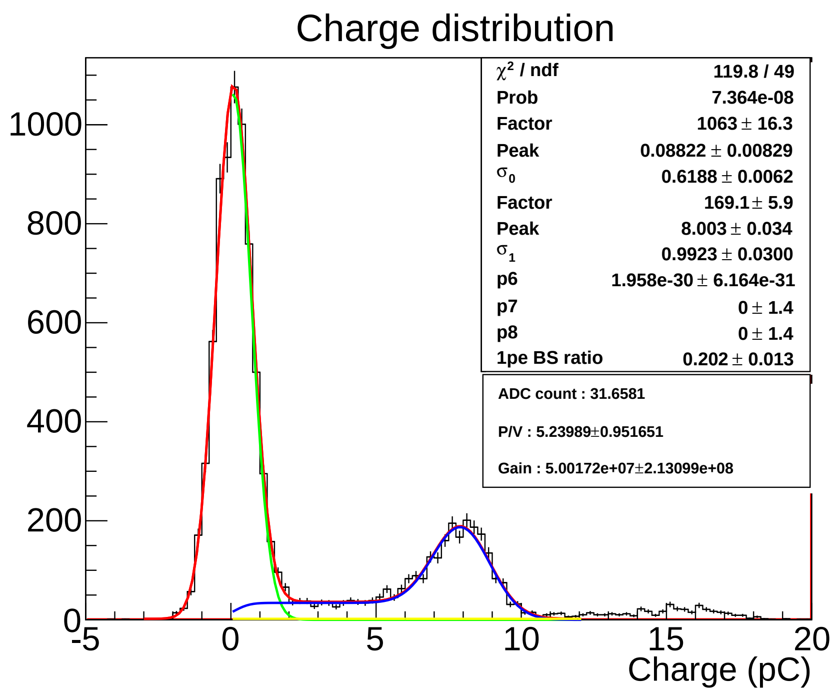

Figure 4.8: Single photoelectron distribution in charge.

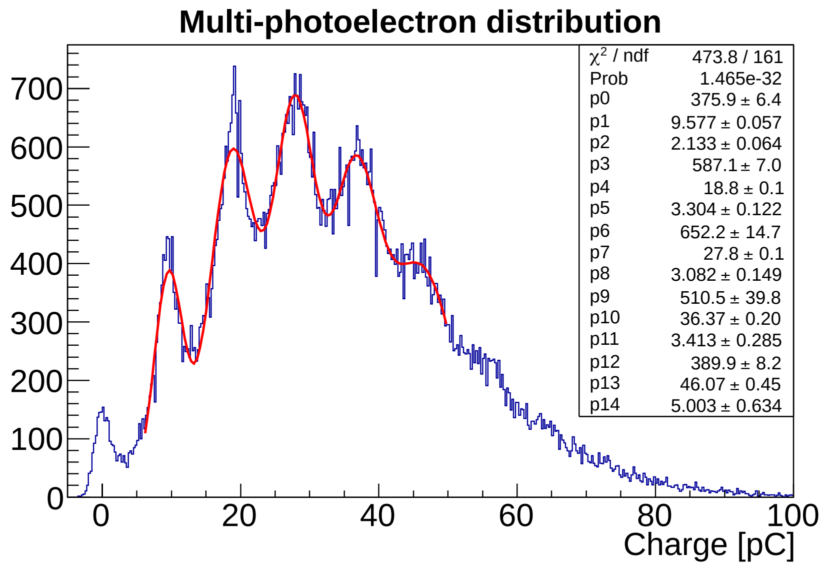

Figure 4.9: Multi-photoelectron distribution in charge.

preamplifier. It will be improved in the next version of the preamplifier.

4.7 Stability of gain

We measure the stability of gain of 8-inch HPD by continuously measuring the pulse height of the output using an oscilloscope. Figure 4.11 shows the measured stability. The horizontal axis shows the time from enabling the HV and the vertical axis shows the pulse height normalized to its average. We can see the gain is stable within ± 0.5 % fluctuation in 50 hours.

4.8 Linearity

Linearity is measured by varying the input light intensity using PLP and VME ADC. We use an APD module (Hamamatsu C5331-11) as a light intensity monitor. Figure 4.12 shows the output charge as a function of the number of the input photoelectrons. The number of the input photoelectron is estimated from the ADC count of APD normalized to the value when the light intensity is single photoelectron level for HPD. Linearity holds up to around 60 photoelectrons, which is limited by the saturation of the preamplifier. This is worse than Super-K PMT, whose output is linear up to 1,000 photoelectrons. This output limit of HPD comes from the rated voltage of the preamplifier. The linearity will be improved in a next version of the preamplifier.

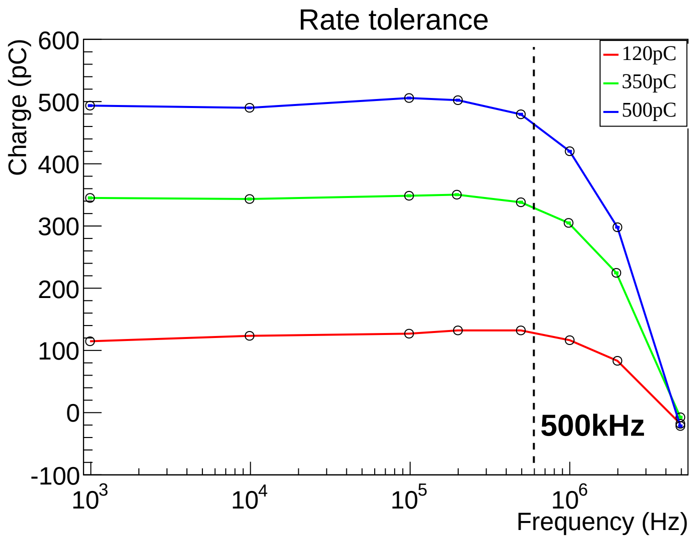

Figure 4.10: Output charge of 8-inch HPD as a function of input light frequency with three different light intensity.

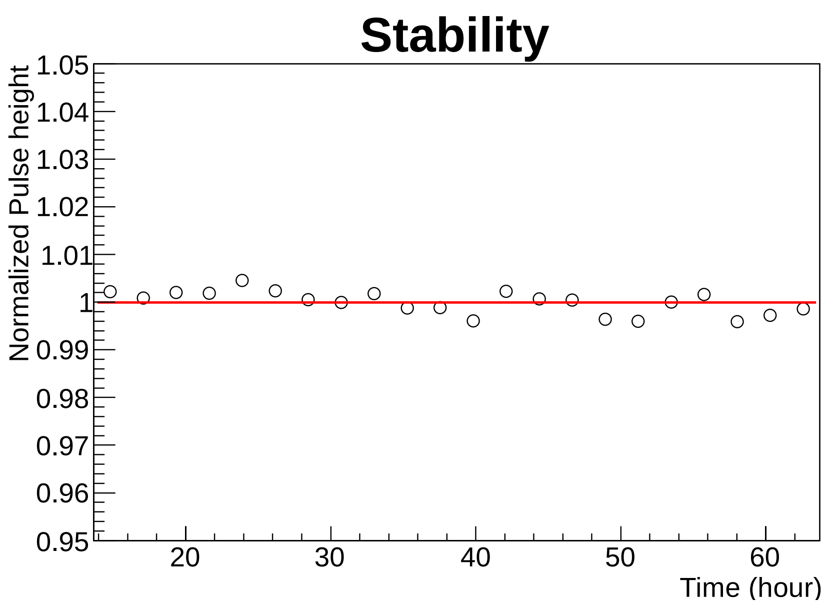

Figure 4.11: Normalized pulse height vs. time.

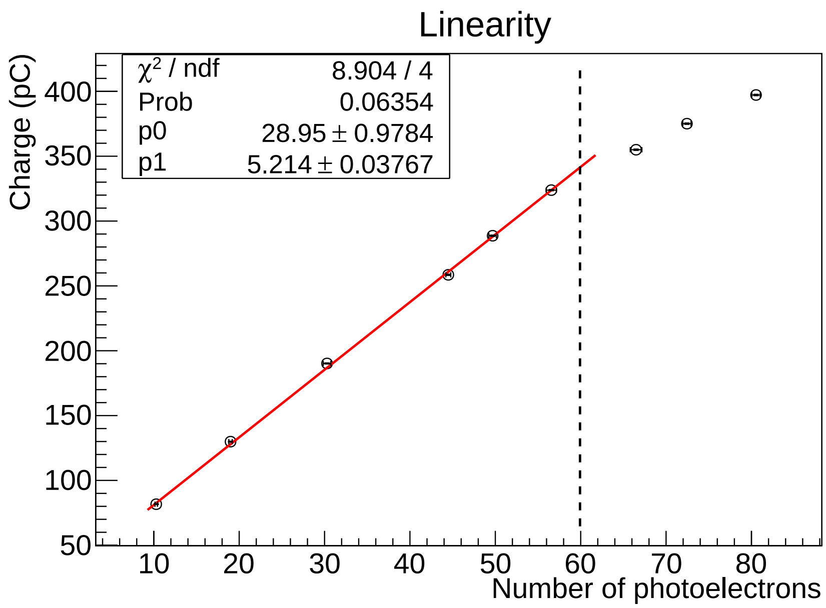

Figure 4.12: Charge vs. number of photoelectrons.

4.9 Response uniformity

The setup for response uniformity measurement is shown in Fig. 4.13. Uniformity is measured by changing the position of the optical fiber, attached onto the photocathode. We set the input light intensity to larger than 10 photoelectrons which is regarded as Gaussian distribution in charge and maintain the intensity during this measurement. A 1-inch PMT (Hamamatsu H7415) is employed as a light intensity monitor and an HPD is placed in a μ-metal shielding box to prevent an effect of the terrestrial magnetism. The HV of each HPD and PMT is turned off when we open the shielding box. After 1 min from switching on the HV, each data taking is started. Figure 4.16 and 4.17 show the gain uniformity over the photocathode along the X and Y-axis respectively. Relative gain is defined by (HPD mean charge (pC))/(monitor PMT mean charge (pC)). Relative gain is uniform from center to 560 mm within 10 %. We also measured the HV dependence of gain uniformity along the Y-axis shown in Fig. 4.18. The response uniformity is independent of the HV.

4.10 Summary and next prototype of HPD

We have confirmed basic performance of 8-inch HPD. HPDs satisfy some of the requirements to Hyper-K photosensor. HPDs have enough low dark rate, better

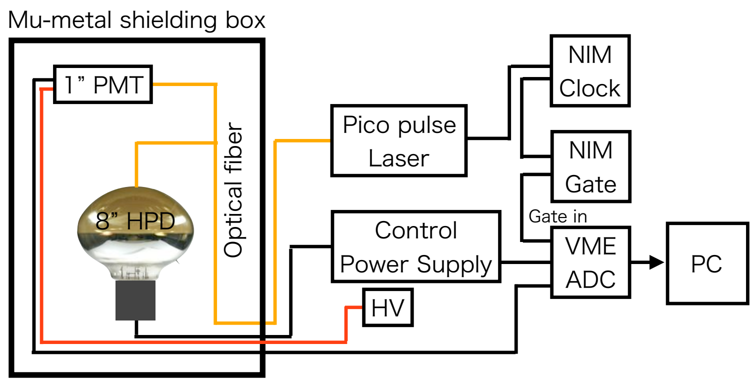

Figure 4.13: Schematic view of the measurement setup of response uniformity.

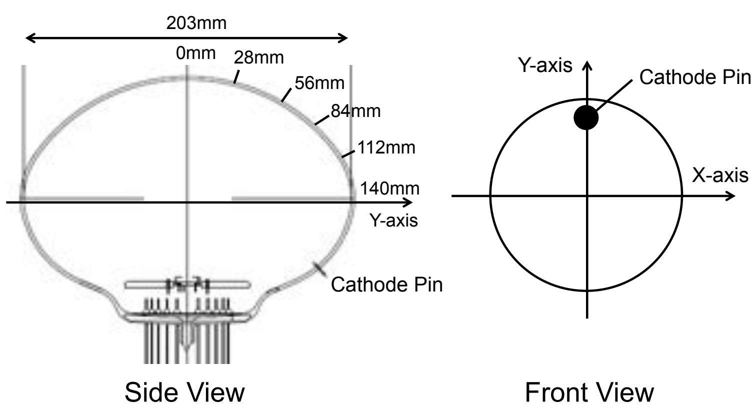

Figure 4.14: Definition of the X and Y-axis and position of the optical fiber.

Figure 4.15: Picture of the response uniformity measurement setup.

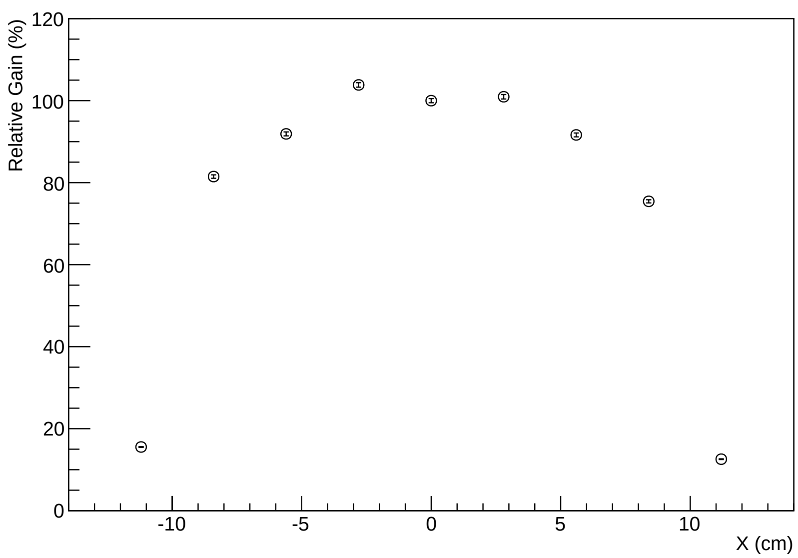

Figure 4.16: Response uniformity along the X-axis.

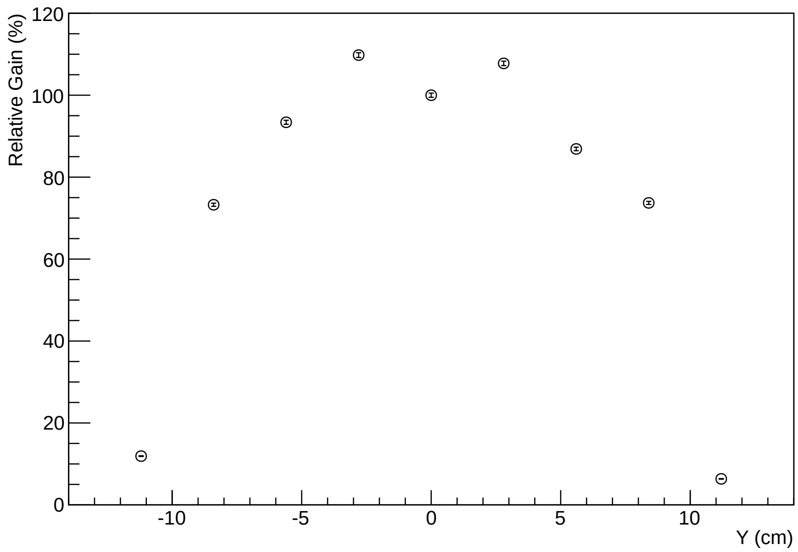

Figure 4.17: Response uniformity along the Y-axis.

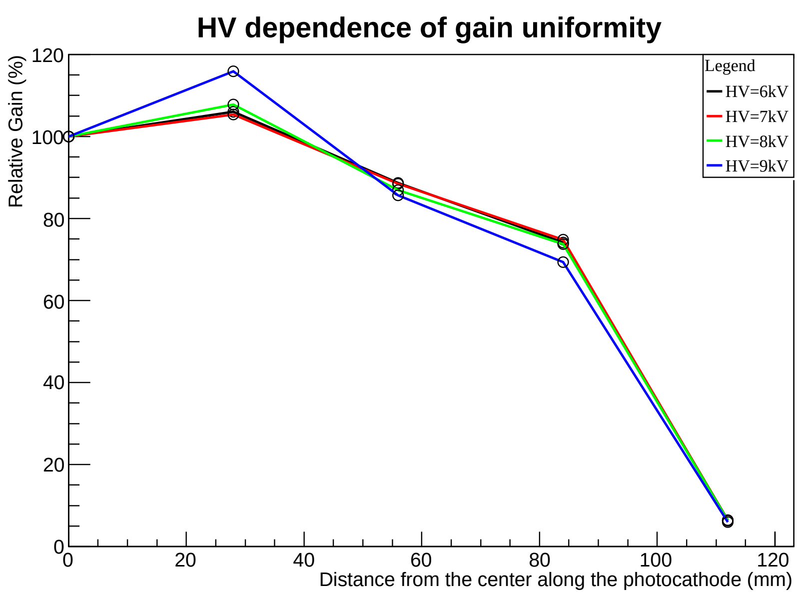

Figure 4.18: HV dependence of response uniformity along the Y-axis.

timing resolution and single photoelectron resolution. But the rate tolerance and the linearity of the current version of the 8-inch HPD do not satisfy the requirements. These limitations come from the specification of the preamplifier. We will improve the preamplifier to satisfy the requirements in the future version of 8-inch and 20-inch HPD.

Chapter 5

Test in the water Cherenkov detector

We have confirmed that the 8-inch HPD has good performance in Chapter 4. As the next step of photosensor R&D, we measure the performance as the sensor for a water Cherenkov detector and the stability using a newly constructed 200-ton water Cherenkov detector. In this chapter, we report the purpose of the test in the water tank, some preparation before installation, sensor installation, the measurement in the tank and its calibration.

5.1 Overview

HPD and the high-QE R3600 have never been used in a water Cherenkov detector. To ensure the usability of these two, we evaluate the performance in a water tank as a sensor for a water Cherenkov detector. We also evaluate the long term stability of HPD and the high-QE R3600. We plan to perform the same test for 20-inch HPD and 20-inch box&line dynode type PMT when they become available.

In Kamioka mine, there are a 200-ton water tank and a water circulation system prepared for another experiment, EGADS (Evaluating Gadolinium's Action on Detector System) experiment (Fig. 5.1) [15]. We use this 200-ton tank for the test of our new photosensors in a water Cherenkov detector. The tank can accommodate up to 240 photosensors in total. We install eight 8-inch HPDs, five high-QE R3600s and 227 normal-QE R3600s into the tank. Then, we evaluate the performance of each photosensor and start the long term stability in the same experimental environment and condition. The test in the water Cherenkov detector will continue for $1 \sim 2$ years.

Before putting inside the water tank, we check the durability, short term stability and operation capability in water of HPD at first. Then we calibrate the gain of the 8-inch HPDs and high-QE R3600s. After that, we install 240 photosensors into the tank. We present the calibration and the first data after

Figure 5.1: Picture of 200-ton tank (EGADS tank).

installation into the tank.

5.2 Pre-test

Before installation, we checked that HPDs have enough durability and no problem to be used in water.

5.2.1 Durability test of the 8-inch HPD

To verify the durability of HPDs, a power cycling test is conducted. We install eight 8-inch HPDs into the tank. Assuming that we will switch on/off 10 times for each HPD in one day during 1 year, HPDs are required to have a durability which means HPD is not breakdown by 30,000 times of HV on/off. Figure 5.2 shows a setup for the durability test. We switch on/off the enable line of a HPD 30,000 times via a mechanical relay board. One cycle takes 20 seconds, 10 sec for enable on and 10 sec for enable off. We operate HPDs over one month in total. Through these tests, there was no breakdown of HPD. We conclude that HPDs have enough durability to be used for the test in the EGDAS tank.

5.2.2 Soak test of the 8-inch HPD

Because HPDs use higher voltage than R3600, we need to check the safety of use of HPDs in water. Figure 5.3 shows the setup for the soak test. We operate

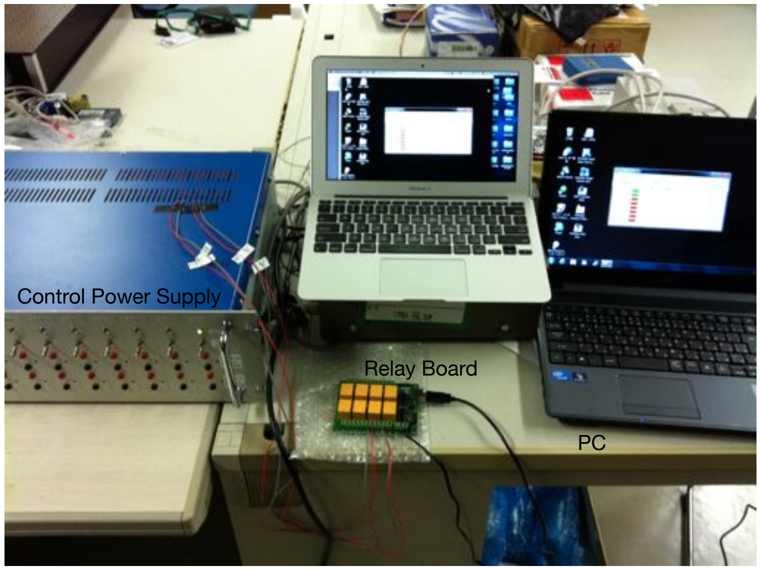

Figure 5.2: Setup for the durability test.

HPDs in water drum for 10 hours one by one. We check the leak current which flows from HPD to ground using a clamp meter (HIOKI 3276) as shown in Fig. 5.4. During the soak test, we have no trouble and observe no leak current.

5.2.3 Pre-calibration

We measure the gain curve of HPDs by the same setup shown in Fig. 4.2. Because the accuracy of the gain measurement is better with a higher output charge, the input light intensity is set to many photoelectrons level. We measure the output charge of HPD with varying the AD bias voltage with fixed HV of 8 kV. The output is scaled the single photoelectron equivalent charge using a separately measured single photoelectron charge for one voltage setting. The gain curves of HPDs are shown in Fig. 5.5.

Using the gain curves, the gain of HPDs is adjusted to 8.2 pC/photoelectron which corresponds to $\sim$13 mV of pulse height within $+1.2\,\%/-2.8\,\%$ (Fig. 5.6). The gain of high-QE R3600s and normal ones are also calibrated as shown in Fig. 5.7. The P/V ratio of each photosensor is measured with the calibrated AD bias voltage as shown in Fig. 5.8. We can see the P/V ratio of HPDs are greater than that of PMTs. The P/V of high-QE R3600s are same level compared with that of normal-QE R3600s. We also measure the dark rate of each photosensor with the calibrated AD bias voltage as shown in Fig. 5.9. The dark rate of eight HPDs are comparable with the normal-QE R3600s. The dark rate of the high-QE R3600 are a bit larger than that of the normal ones.

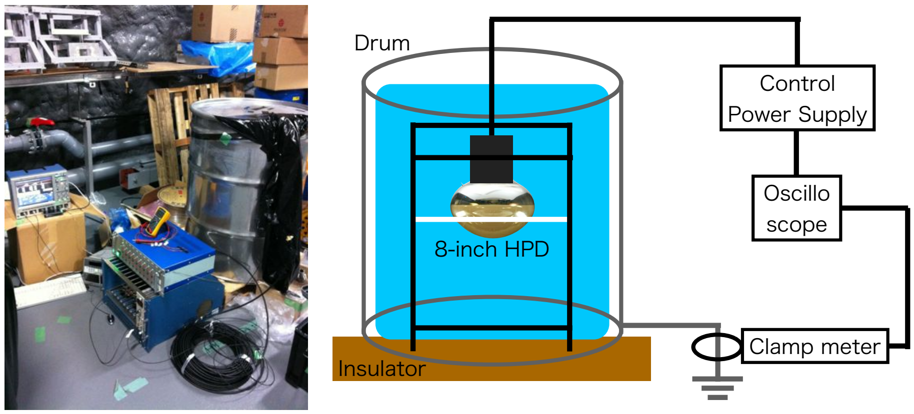

Figure 5.3: Setup for the soak test.

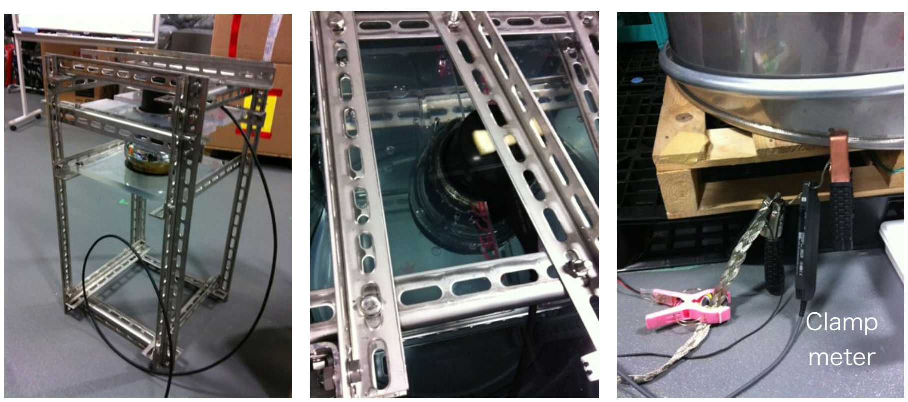

Figure 5.4: Pictures of the jig for HPD (left), HPD in water drum (center) and Clamp meter (HIOKI 3276) (right).

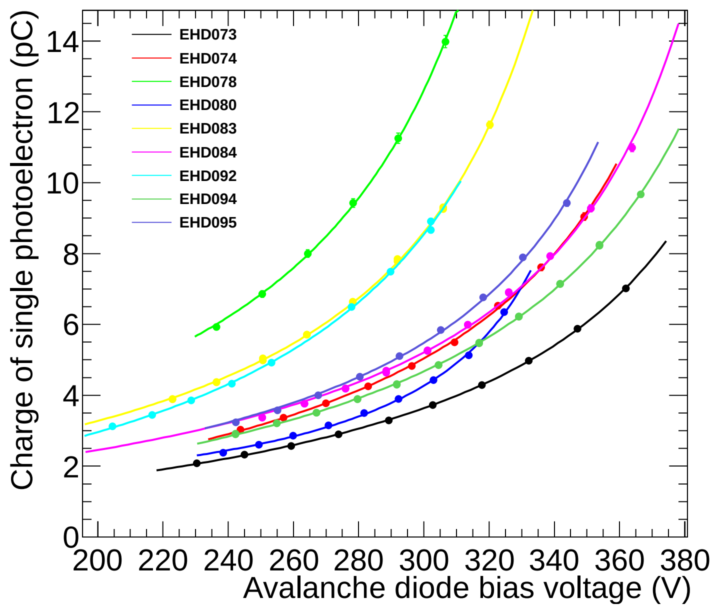

Figure 5.5: Variation of the gain curve of HPDs.

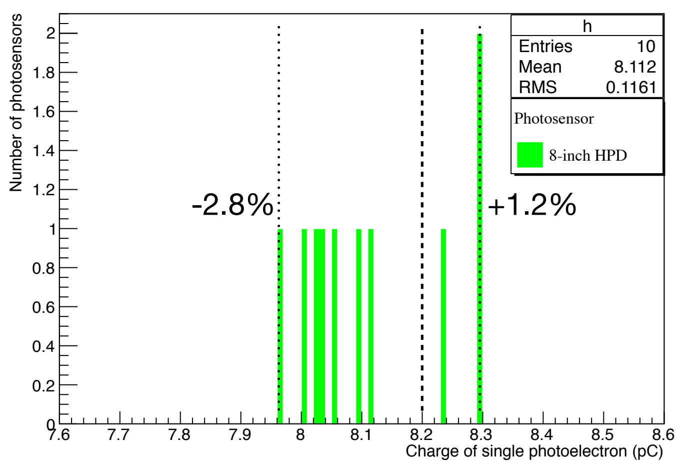

Figure 5.6: Charge of single photoelectron of ten HPDs.

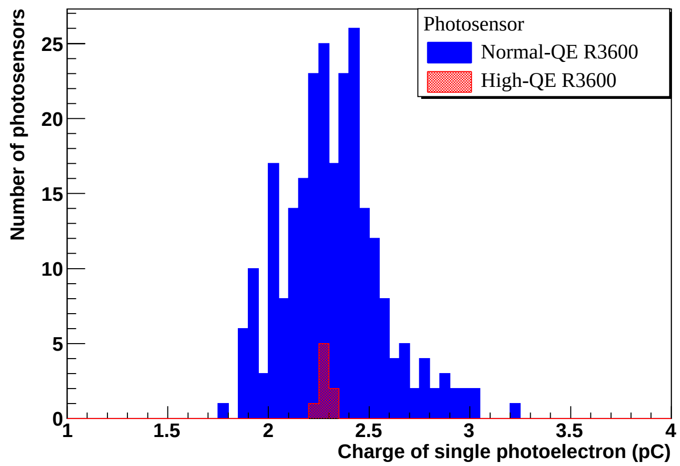

Figure 5.7: Charge of single photoelectron of PMTs.

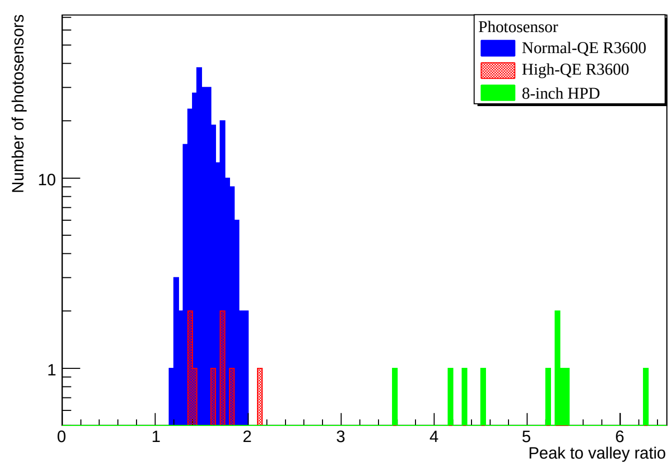

Figure 5.8: P/V ratio of each photosensor.

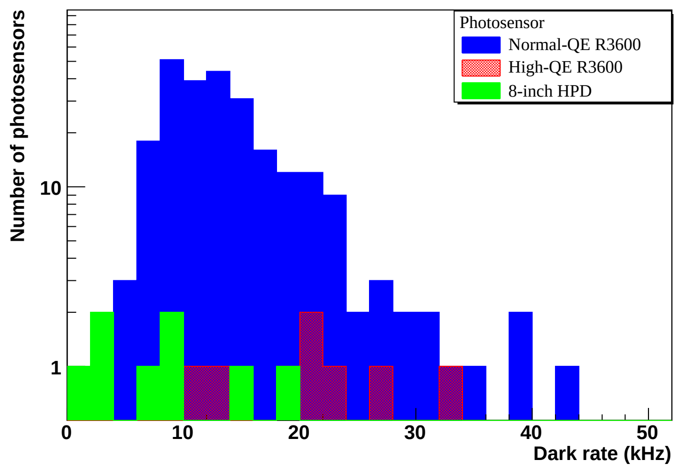

Figure 5.9: Dark rate of each photosensor.

5.3 Installation

The installation of photosensors into the EGADS tank is conducted from July 16th to August 13th in 2013. Figure 5.10 shows the map where our photosensors are placed. First we check the signal of the photosensor using an oscilloscope, and then clean up and attach the jig to fix the photosensor on the tank. After that we install the photosensor into the tank and connect the cable of the photosensor to the cable connected into the DAQ board. For DAQ system, we use the ATM board which is used in previous Super-K. Finally we check the signals of each photosensor one by one using an oscilloscope (Fig. 5.11). We successfully mounted photosensors to the 200-ton water Cherenkov tank in August (Figs. 5.12 and 5.13).

A few days after filling water into the tank, one HPD (No. 74) became unoperatable. We think that this trouble was caused by malfunctioning of the HV module. The development of more robust HV module is an urgent issue of the HPD R&D. There is no further breakdown of photosensors. Seven HPDs are available for the long term test.

5.4 DAQ system

In this section, we show the DAQ setup for the test in the water tank.

The control power supply for eight HPDs, power supply for 232 PMTs, ATMs and some electronics are shown in Fig. 5.14. The power supply of the high-QE R3600s and that of the normal ones are common. One ATM has 12 channels and we employ 22 ATM boards. When the signal which exceeds the

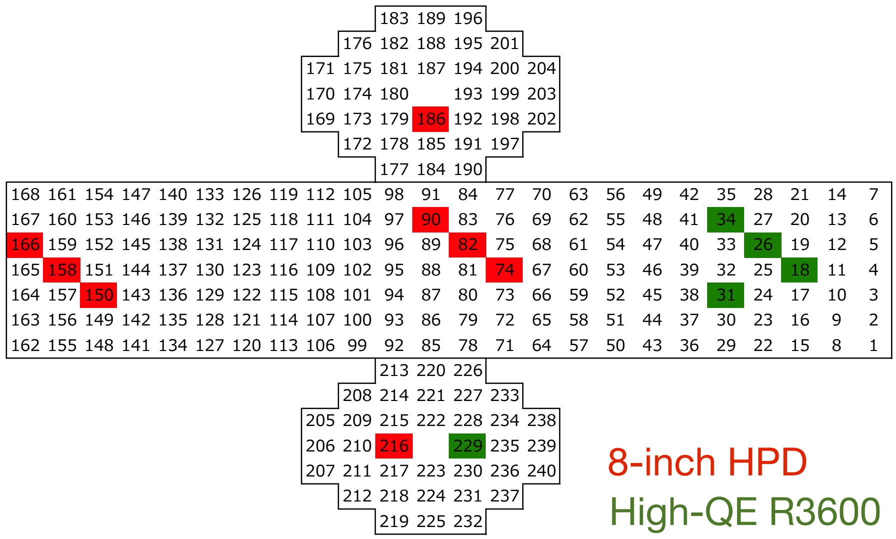

Figure 5.10: Photosensor map.

threshold voltage is inputted into an ATM board, it integrates the charge of the input signal with 400 ns window and records the timing of the signal. We can trigger the DAQ by using some electronics which is placed under the control power supply. Figure 5.15 shows the back plane of the control power supply. The 70 m cables coming from inside the tank are connected to the control power supply and the ATM boards.

To monitor the HPDs, we set two voltage logger, a temperature logger and a relay board as shown in Fig. 5.16. The voltage logger records the control voltage of the HV and AD bias voltage to monitor the stability of the HV and AD bias voltage. Four HPDs have Pt100 as a temperature sensor inside the module. The temperature logger records the temperature inside the HPDs to study the temperature dependence of gain. To control remotely the enable of HPDs, we use the relay board. In emergency situation, we can immediately disable the HPDs. Two connectors relay the connection each monitor module to the control power supply.

After establishment of DAQ setup, we conduct the noise reduction. We found that the periodic noise in the signal of HPDs come from a VME module. Attaching a ferrite core to an AC cable of a VME crate, the noise is reduced. We also improved grounding to reduce the noise level.

Figure 5.11: Procedure of installation.

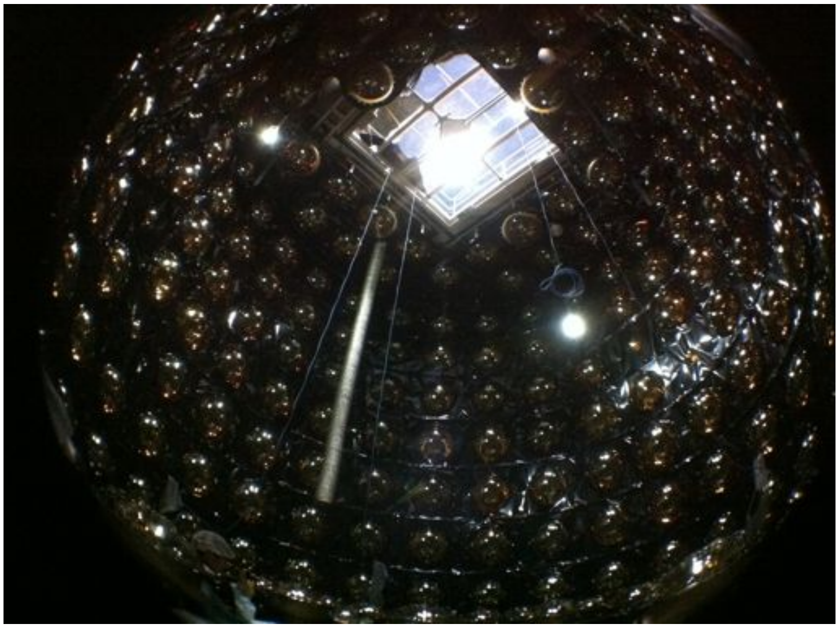

Figure 5.12: Picture when the installation completed.

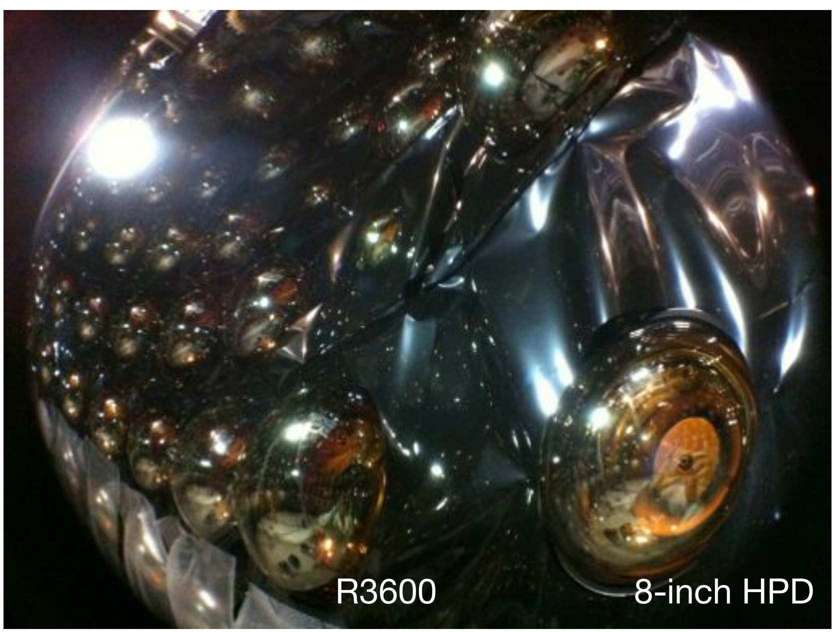

Figure 5.13: 8-inch HPD with R3600s in tank.

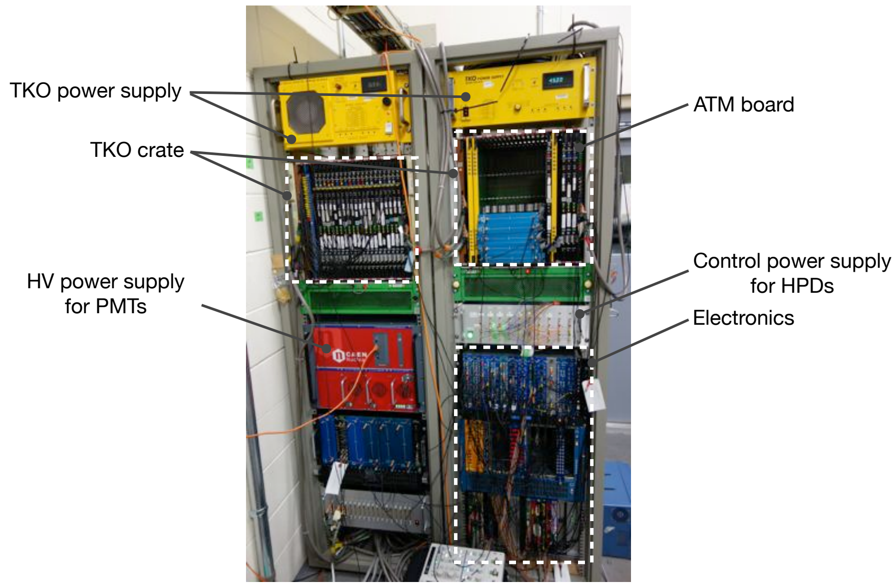

Figure 5.14: Picture of the front view of the electronics.

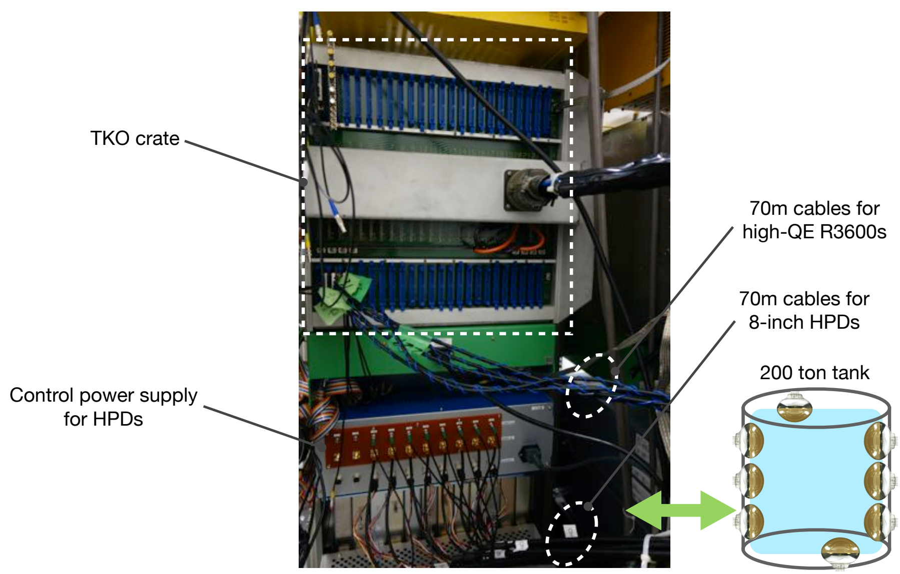

Figure 5.15: Picture of the back view of the electronics.

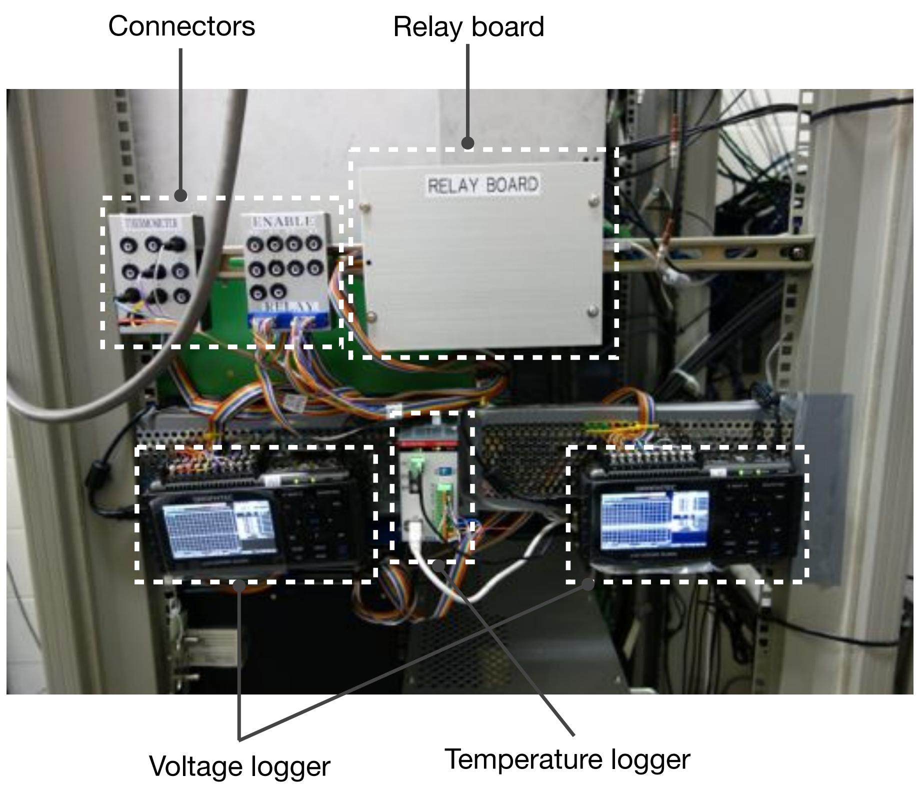

Figure 5.16: Picture of the side view of the electronics.

5.5 The measurement in the water tank

After the installation, we measured the single photoelectron signal and the dark rate of photosensors and calibrated the gain of HPDs. The cosmic muon-like events observed in the tank are shown in Figs. 5.17. The EGADS detector works as a water Cherenkov detector. Figure 5.18 shows a setup for the measurement using a laser diode (OPG-1000-NIM, $\lambda = 405$ nm, pulse width (70∼80 ps)). The light emitted by the laser diode is diffused uniformly inside the tank through a diffuser ball. By changing the light intensity of the laser diode, we measure the charge of the single photoelectron of 8-inch HPDs. The threshold of all HPDs is fixed at -1.5 mV which corresponds to about 1/5 photoelectron. Figure 5.19 shows a result for one HPD (No. 82). The single photoelectron resolution is about 30 % in sigma, while 40∼50 % in case of PMTs. The difference between the single photoelectron resolution 12 % as shown in section 4.5 and this value 30 % comes from the difference of the gate width and the existence of the 70 m cable. The multi photoelectron distribution measured with an HPD is shown in Fig. 5.20. We can see clear separation of photoelectrons up to four photoelectrons. Figure 5.21 shows the photoelectron resolution defined by sigma/mean of nth photoelectron peak as a function of the number of photoelectrons. The photoelectron resolution becomes better with the larger number of photoelectrons.

We calibrate the gain of HPDs using the same system of Fig. 5.19. The target value is 7.6 pC/photoelectron. The gain is adjusted to 7.6 pC/photoelectron within 4.7 % (Fig. 5.22).

After the calibration, we measure the dark rate of all HPDs using the VME scaler. The result is shown in Fig. 5.23. The single photoelectron is around 8 mV. Channel 0 is for the dead channel as described in previous section. Channel 1 and 2 have relatively high dark rate. We suspect that these high dark rate are caused by some HV module issues. The other five HPDs have the dark rate less than 2 kHz at 0.5 photoelectron threshold. Figure 5.24 shows the comparison of the dark rate of an HPD (No. 150) between before and after the installation into the water tank. At 0.5 photoelectron level, the dark rate taken in May 22th, October 12th and November 21th are 2 kHz, 0.6 kHz and 0.4 kHz, respectively. Because of the low temperature in the tank and closing the tank for two months, the dark rate decreases. Figure 5.25 and Fig. 5.26 show the dark rate of the high-QE R3600s and the normal ones. At this time, we use an amplifier with a gain of 4.4. The dark rate of the high-QE R3600s at around 10 mV which corresponds to 0.25 photoelectron is comparable to that of the normal ones.

5.6 Summary and future plan

The installation of photosensors is successfully completed in August. The measurement in the water tank shows that HPDs have better single photoelectron resolution, clear separation of photoelectrons and enough low dark rate in the tank.

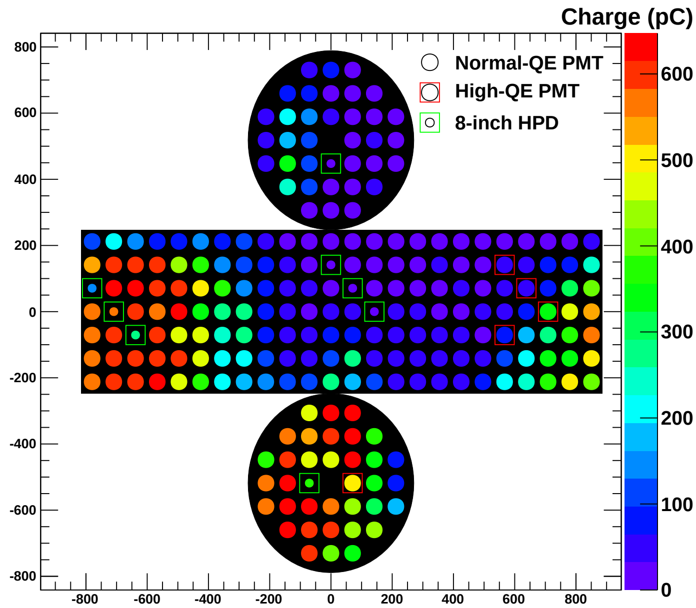

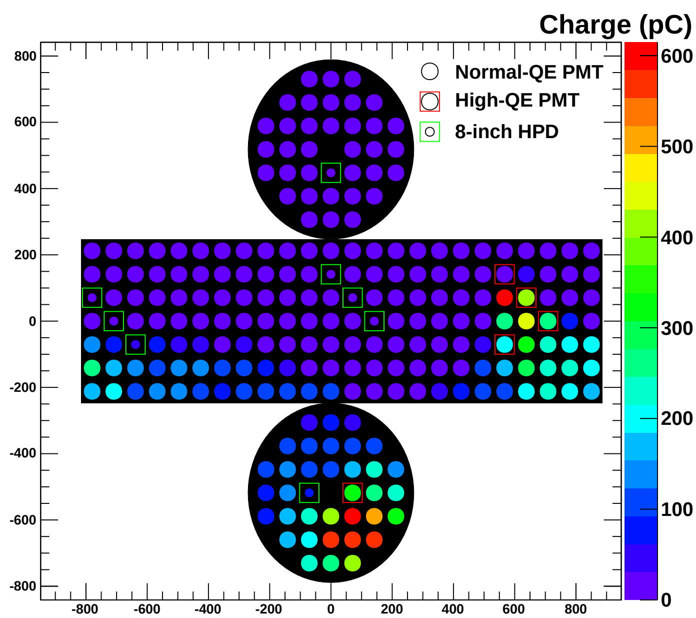

Figure 5.17: Cosmic muon-like event. The color shows the charge of the hit. The warm color is for large charge. The cold color is for small charge.

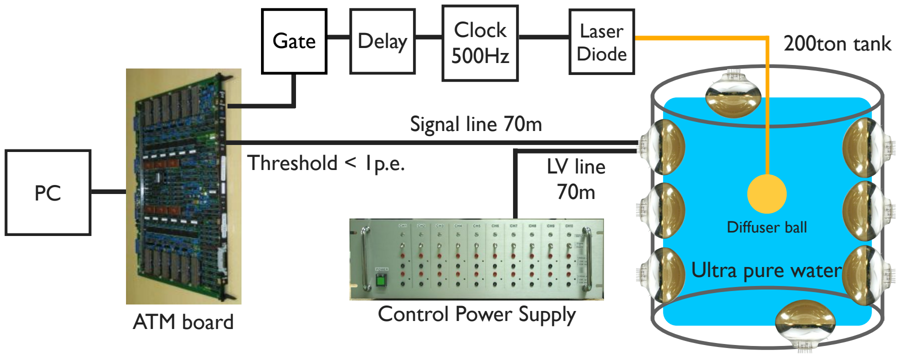

Figure 5.18: Setup for the single photoelectron measurement in 200-ton tank.

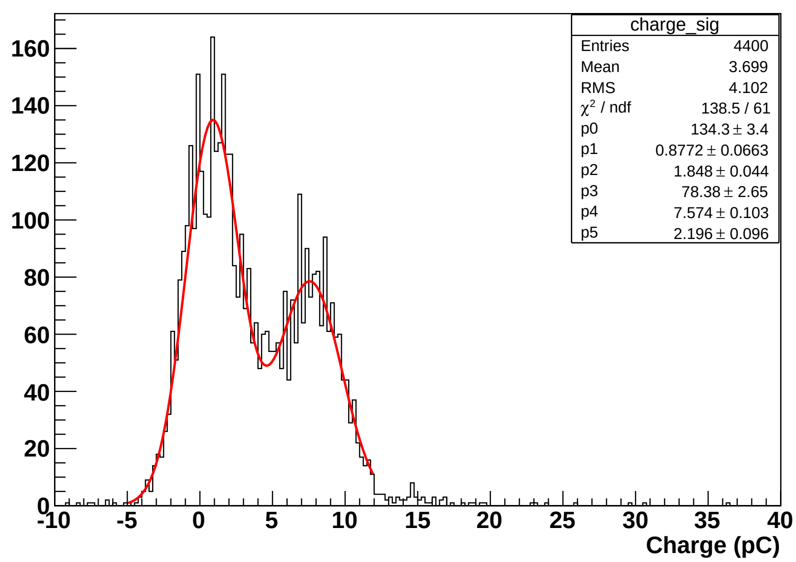

Figure 5.19: Single photoelectron distribution of an 8-inch HPD measured in EGADS tank.

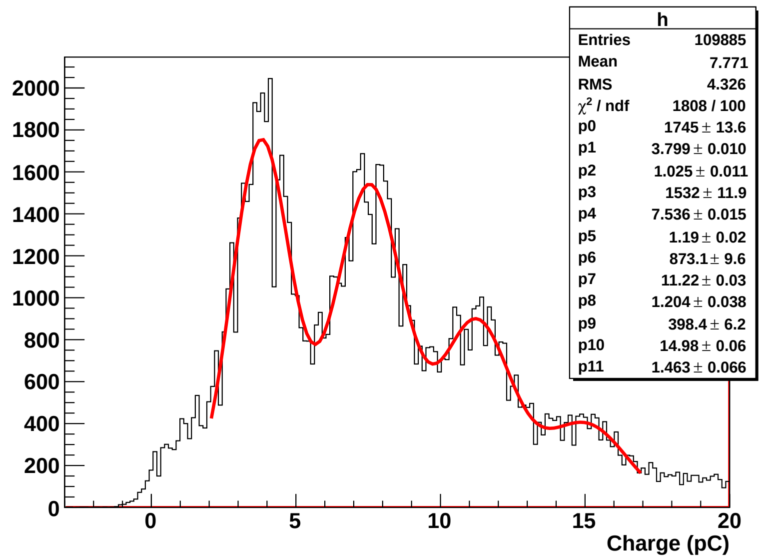

Figure 5.20: Multi photoelectron distribution of an 8-inch HPD.

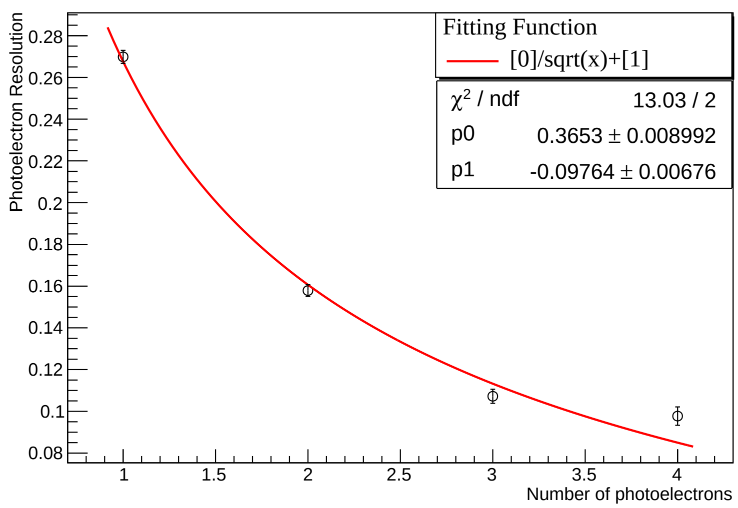

Figure 5.21: Photoelectron resolution of an 8-inch HPD as a function of number of photoelectrons.

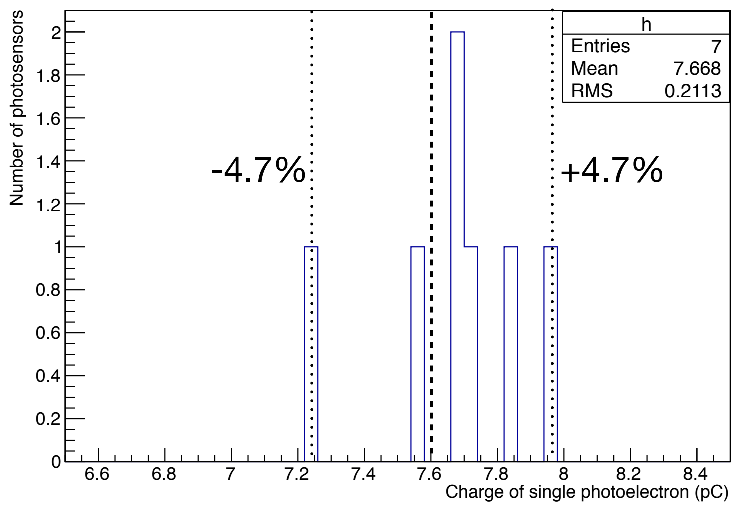

Figure 5.22: Single photoelectron peak values of HPDs after single photoelectron calibration.

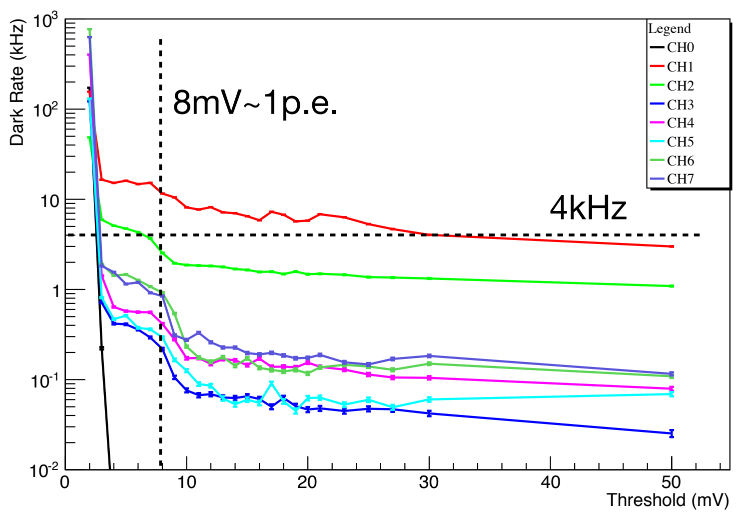

Figure 5.23: Dark rate distribution of eight 8-inch HPDs measured in EGADS tank. Ch 0 is for a broken HPD.

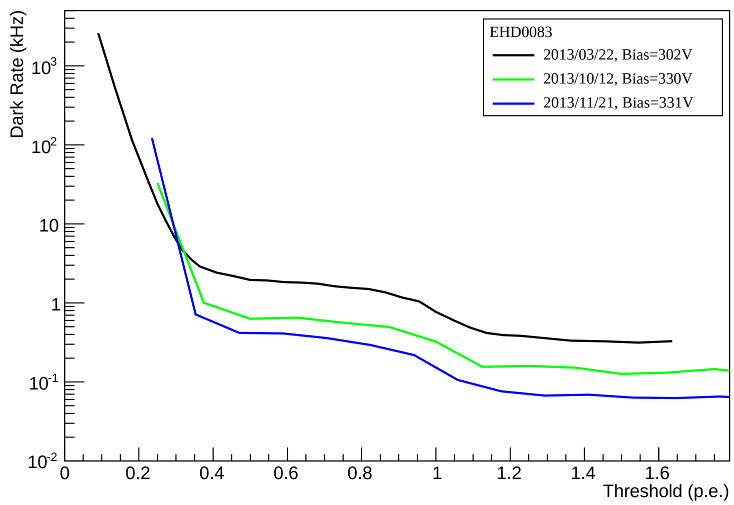

Figure 5.24: Comparison between before after the installation.

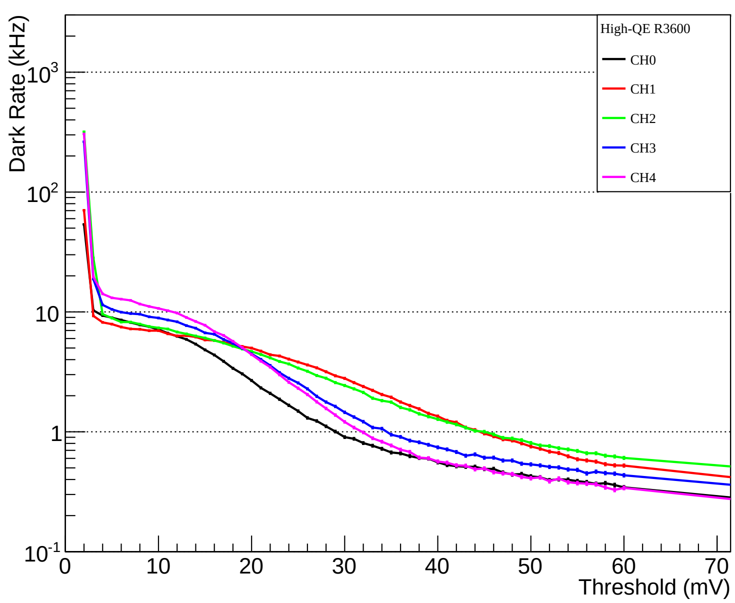

Figure 5.25: Dark rate of five high-QE R3600 with an amplifier $\times$ 4.43.

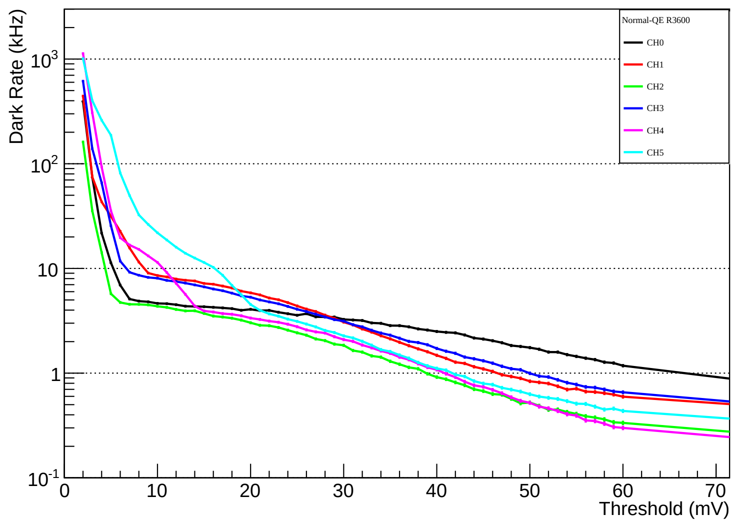

Figure 5.26: Dark rate of six normal-QE R3600 with an amplifier × 4.43.

These are the first measurement of the 8-inch HPD and the high-QE R3600 in the water Cherenkov detector. We calibrate the gain of HPDs. We will start the long term testing in February 2014. Comparing with the normal-QE R3600s, we evaluate the usability of HPDs and high-QE photocathode in the long term testing. The first version of prototypes of 20-inch HPD and 20-inch box&line dynode type PMT will be available in early 2014 (Fig. 5.27). We select the photosensor for Hyper-K during 2016.

Figure 5.27: Picture of 20-inch HPD and 20-inch box & line dynode type PMT. Courtesy of Hamamatsu Photonics K.K.

Chapter 6

Summary and future prospects

6.1 Summary

We have developed the prototype of 8-inch HPD. The 8-inch HPD satisfies some requirements to photosensors in Hyper-K. It has a simple structure, large photosensitive area, dark rate of 2 kHz at 0.5 photoelectron, timing resolution of 1.2 ns and single photoelectron resolution of 12 %. But some requirements such as the linearity and the rate tolerance do not satisfy the requirements and need improvement. In order to install the HPD into the water Cherenkov tank, we confirmed the durability and safety operation in water. We installed eight 8-inch HPDs, 5 high-QE R3600s and 227 normal-QE R3600s. The single photoelectron resolution of the 8-inch HPD is better than R3600 in the tank. The dark rate of the 8-inch HPD in the tank decreased compared with the measurement before installation. One HPD was broken a few days after filling the water. We suspect that the problem is caused by the HV module trouble. We also have developed the high-QE R3600. The single photoelectron resolution and P/V ratio of the high-QE R3600 are the same that of the normal-QE R3600. The dark rate of the high-QE R3600 is comparable to that of the normal-QE R3600.

6.2 Future prospects

The major topics of R&D of HPD are the R&D of 20-inch HPD, the test in the water Cherenkov detector and the improvement of the preamplifier and the HV module. The first version of prototype of 20-inch HPD will be available in early 2014. The test in the water Cherenkov detector will start in early 2014. We are developing the next version of the preamplifier to make the best performance of HPD. To ensure that HPD is useful to use in a water Cherenkov detector, the stable operation of the HV module is the key.

Acknowledgements

I would like to express my great appreciation to my supervisor Prof. Masashi Yokoyama for his overall support. Through discussion with him, I could understand my work more deeply. Without him advices, this thesis would not exist.

Many thanks to Dr. Yasuhiro Nishimura and Seiko Hirota. They taught me how to operate HPD, how to take and analyze data. Whenever I am preparing a transparency, they gave me many comments even if it is midnight.

I must thank to Prof. Masato Shiozawa, Prof. Yoshinari Hayato, Dr. Shoei Nakayama, Dr. Hidekazu Tanaka, Prof. Tsuyoshi Nakaya, Prof. Masahiro Kuze and Dr. Akimichi Taketa for their guidance and supervision. I also want to thank Dr. Tomonobu Tomura who graduated my laboratory, Kazuki Iyogi, Hiroyoshi Uchida, Shota Takahashi, Kunxian Huang, Hiroki Takiya, Tadashi Hosokawa, Osamu Takachio, Yuki Nakano, Naoya Oka, Katsuma Nakagawa, Yuto Haga, Isao Kametani, Keiji Tateishi, Yosuke Ohnishi, Asato Orii, Tateo Nakajima, Masatoshi Kobayashi, Yuji Okajima and Zhi Li for my happy life in Kamioka.

I am indebted to the members of Hamamatsu Photonics K.K. Dr. Yoshihiko Kawai, Takayuki Ohmura and Masatoshi Suzuki, especially for the development of HPD and high-QE PMT.

I need to thank to the members of EGADS experiment Prof. Masayuki Nakahata, Prof. Mark Vagins, Prof. Yusuke Koshio, Dr. Motoyasu Ikeda, Dr. Astuko Kibayashi, Dr. Takatomi Yano and Takaaki Mori. They approved to install our photosensors into the EGADS tank and helped us to take data in the tank.

My appreciation also goes to the members of Aihara/Yokoyama laboratory Prof. Hiroaki Aihara, Dr. Yoshiyuki Onuki, Dr. Denis Epifanov, Sogo Mineo, Clement Ng, Yasutaka Kanazawa, Nobuhiro Shimizu, Taichiro Koga, Junya Sasaki and Yifan Jin for my fruitful life in Hongo. I would like to thank Kuniko Kono who supports my laboratory for her fantastic assist. I would also like to appreciate Dr. Akito Kusaka, Dr. Hiroyuki Nakayama and Jiayin Wang for their research and development of HPD.

Finally, I would like thank to my family and all my friends.

Bibliography

[1] K. Abe, T. Abe, H. Aihara, Y. Fukuda, Y. Hayato, et al. Letter of Intent: The Hyper-Kamiokande Experiment — Detector Design and Physics Potential —. 2011.

[2] Y. Fukuda et al. Evidence for oscillation of atmospheric neutrinos. Phys.Rev.Lett., 81:1562–1567, 1998.

[3] K. Abe et al. Observation of Electron Neutrino Appearance in a Muon Neutrino Beam. 2013.

[4] F.P. An et al. Observation of electron-antineutrino disappearance at Daya Bay. Phys.Rev.Lett., 108:171803, 2012.

[5] J.K. Ahn et al. Observation of Reactor Electron Antineutrino Disappearance in the RENO Experiment. Phys.Rev.Lett., 108:191802, 2012.

[6] Y. Abe et al. First Measurement of θ_{13} from Delayed Neutron Capture on Hydrogen in the Double Chooz Experiment. Phys.Lett., B723:66–70, 2013.

[7] Ziro Maki, Masami Nakagawa, and Shoichi Sakata. Remarks on the unified model of elementary particles. Prog.Theor.Phys., 28:870–880, 1962.

[8] R.B. Patterson. The NOvA Experiment: Status and Outlook. Nucl.Phys.Proc.Suppl., 235-236:151–157, 2013.

[9] K. Hirata et al. Observation of a Neutrino Burst from the Supernova SN 1987a. Phys.Rev.Lett., 58:1490–1493, 1987.

[10] R.M. Bionta, G. Blewitt, C.B. Bratton, D. Casper, A. Ciocio, et al. Observation of a Neutrino Burst in Coincidence with Supernova SN 1987a in the Large Magellanic Cloud. Phys.Rev.Lett., 58:1494, 1987.

[11] E.N. Alekseev, L.N. Alekseeva, I.V. Krivosheina, and V.I. Volchenko. Detection of the Neutrino Signal From SN1987A in the LMC Using the Inr Baksan Underground Scintillation Telescope. Phys.Lett., B205:209–214, 1988.

[12] Y. Fukuda et al. The Super-Kamiokande detector. Nucl.Instrum.Meth., A501:418–462, 2003.

[13] Hirokazu Ikeda, Masaki Mori, Tohru Tanimori, Keni-ichi Kihara, Yoichiro Suzuki, et al. Front end hybrid circuit for Super-Kamiokande. Nucl.Instrum.Meth., A320:310–316, 1992.

[14] A. Suzuki, M. Mori, K. Kaneyuki, T. Tanimori, J. Takeuchi, et al. Improvement of 20-inch diameter photomultiplier tubes. Nucl.Instrum.Meth., A329:299–313, 1993.

[15] Takatomi Yano. Status of the Gadolinium project for Super-Kamiokande. PoS, ICHEP2012:382, 2013.